INVESTIGATION OF RADON, CHROMIUM, ZINC AND IRON IN DRINKING WATER SOURCES AND ITS HEALTH IMPACTS IN THE SOUTH OF KARAK CITY, KHYBER PAKHTUNKHWA, PAKISTAN

By

Sarmad Aali Shan Haider

Department of Earth and Environmental Sciences Bahria University, Islamabad Pakistan

2024

Investigation Of Radon, Chromium, Zinc And Iron In Drinking Water Sources And Its Health Impacts In The South Of Karak City, Khyber Pakhtunkhwa, Pakistan

A thesis submitted to Bahria University, Islamabad in partial fulfilment of the requirement for the degree of M.S in Geology

Sarmad Aali Shan Haider

Department of Earth and Environmental Sciences Bahria University, Islamabad Pakistan

2024

Acknowledgements

I am thankful to Almighty Allah, the most beneficent and the most merciful, for His boundless blessings with which we qualified to pursue this study. I would like to express my deepest gratitude to Dr. Mumtaz Ali Khan, my thesis supervisor, for his invaluable guidance, support, and encouragement throughout the research process. Their expertise, patience, and unwavering commitment have been instrumental in shaping this thesis. I extend my appreciation to the Earth and Environmental Sciences Department, Bahria University, for providing me with the resources and facilities necessary to conduct this research.

Finally, I would like to express my heartfelt gratitude to my family for their unwavering love, encouragement, and understanding. Their support has been a constant source of strength and motivation.

Abstract

This study undertakes a critical examination of groundwater resources in the southern region of Karak district, with a particular emphasis on the concentration levels of radon and heavy metals such as iron, chromium, and zinc. The analysis aims to assess potential health risks associated with these contaminants, employing hazard quotient and daily chronic intake calculations as evaluative metrics. A comprehensive sampling effort yielded 30 water samples for radon analysis and an equal number for the assessment of Fe, Zn, and Cr. Results indicate radon levels in drinking water samples with a mean of 8.4 ± 0.4 Bq l^{-1}, a maximum of 21.3 ± 0.9 Bq l^{-1}, and a minimum of 3.85 ± 0.2 Bq l^{-1}. Iron concentrations ranged from 0.010 ppm to an unspecified upper limit, averaging 0.06837 ppm, while chromium levels spanned from 0.020 ppm to 0.7 ppm, with a mean value of 0.0911 ppm. Zinc concentration fluctuated between 24 ppb and 52 ppb, averaging 39.433 ppb. This research provides critical insights into water quality challenges in the region, serving as a foundational resource for evidence-based policymaking and public health initiatives.

Table of Contents

Chapter 5

Results And Conclusion

Chapter 6

Discussion

List of Figures

List of Tables

CHAPTER 1
INTRODUCTION

1.1 Introduction

Nestled in Pakistan's scenic Khyber Pakhtunkhwa province, Karak is a geological wonderland with immense significance for scientific research and resource exploration. With its strategic location in the country's northwestern part, Karak boasts diverse geological formations, captivating scientists and adventurers alike. Karak offers a captivating journey into the Earth's history and an opportunity to uncover the region's geological treasures from its intriguing rock structures to its rich mineral deposits.

Karak stands out as a densely populated district within the Khyber Pakhtunkhwa province of Pakistan. Encompassing an area of 2,650 square kilometers, the district is divided into three distinct Tehsils: Tehsil Karak, Banda Daud Shah, and Takht-e-Naserati (Ullah et al., 2013). Regarding geology, District Karak boasts four distinct types of rock formations. The Chinji Formation primarily comprises reddish shale and sandstone, while the Nagri Formation is predominantly composed of sandstone with intermittent shale beds. Additionally, the Dhok Pathan formation contains a mix of sandstone, shale, and conglomerates, while the Soan formation is characterized by reddish-brown shale alongside greyish-brown sandstone (Ullah et al., 2013).

Every person should have the fundamental right to fresh and hygienic water (Tahir, 2004; Ilyas et al., 2017). Ensuring access to clean and safe drinking water is a crucial concern in today's world. In general, water sources are broadly classified into surface and subsurface categories, catering to a multitude of purposes such as sanitation, agricultural activities, personal care, and household consumption (Cahill, 2000; Shirley et al., 2000). But the suitability of water for these purposes relies entirely on its quality (Eldon and Bradley, 2004). To be considered suitable and wholesome for consumption, maintaining a balance in both biological and physio-chemical properties is essential. (Rezaee et al., 2001). Elevated levels of certain trace metals like Cr, Pb, Cu, Cd, Ni, and others in freshwater can significantly compromise its quality and pose health risks (Storelli et al., 2005; Zhang et al., 2014).

The presence of radon in the drinking water sources of Karak City has been reported by Khan et al., (2022) that unexpectedly high concentrations of radon (Rn) in soil may be observed, exceeding levels typically associated with uranium decay in the earth. Major migratory pathways for radon are predominantly formed by faults, cracks, and fractures in the bedrock. Several studies have demonstrated that abnormal concentrations of radon are more likely to occur along active faults compared to background levels (Khan et al., 2022). Increased radon gas concentrations near cliffs or steep slopes can be linked to several factors, the migration of radon gas within the fault areas or fluctuations in radon generation influenced by shifts in the near-surface geological layers associated with faults. The findings of Khan et al., (2022) provide substantial indications of convective movement of 222Rn taking place in specific, localized spots along fault lines. Radon has a two-fold impact on human life. It serves as a valuable tool for detecting and forecasting seismic events, volcanic eruptions, fault activity, and hydrological research when present in soil, water, and rocks. Conversely, elevated levels of radon in indoor settings and drinkable water can pose a notable health hazard to people due to its cancer-causing properties. (Khan et al., 2011).

Tube Wells are the only and primary source of drinkable water in the area, although, in certain villages, people rely on pressure pumps, hand pumps, and tube wells for their domestic and drinking water needs. Typically, the sandstones of the Siwalik Group are reported to hold a large amount of water. However, in some locations, the alluvial deposits derived from the Siwalik Group may contain perched water lenses. One notable consideration is that the Siwalik formations, known for their uranium mineralization in certain localities within the region, have a higher likelihood of releasing radon gas into the water sources. This potential presence of radon can pose health hazards for the local population. Furthermore, Water sourced from the natural springs in the region is anticipated to harbor radon, a phenomenon through which radon from deeper formations infiltrates through the faults that are active tectonically. (Khan et al., 2014)

The decay of uranium and thorium within the soils and rocks gives rise to a radioactive gas that is known to be devoid of any color, has no smell, and has no taste called radon gas. It can be liberated into the air and water and can accrue in confined spaces such as homes, mines, and underground caves. As per the UNSCEAR (2008)

report, radon gas and its radioactive isotopes constitute the most substantial share of the annual effective dose from naturally occurring radioactive materials to humans. Radon exists in nature as three well-known isotopes: radon-222 (222Rn), thoron-220 (220Rn), and actinon-219 (219Rn). The isotope exhibiting high prevalence and stability among these is radon-222, which originates from the decay of 238U, an isotope of uranium, representing the bulk, about 99.3%, of the total uranium content in nature. Thoron-220 is naturally generated at the time of the breakdown of 232Th, whereas actinon-219 forms as a result of the decay of 235U (Khattak et al., 2014). The radioactive decay half-life of radon-222 is roughly 3.8 days. During its decay, it emits an alpha particle with an energy of 5.49 meV, giving rise to radioactive daughters in the process (Khattak et al., 2014).

The concentration of radon near the Earth's surface, without the influence of outward gas flow, is primarily determined by the presence of 226Ra. This solid material, 226Ra, exhibits considerable variations in levels across the Earth's surface. Consequently, precise average values for the concentration of radon within the soil, along with its distribution along faults and fractures, remain elusive. To comprehend this phenomenon better, it is crucial to recognize that radon originates from the decay of the 238U decay series. This series also gives rise to various other isotopes with extended half-lives (such as 234U, 226Ra, and 230Th), commonly found in metamorphic rocks, sedimentary, and igneous rocks. This prevalence enables radon to be generated by virtually all kinds of soils and rocks at various depths. (Khan et al., (2022)).

Humans can come into contact with chromium, mainly in its trivalent (III) and hexavalent (VI) forms, which are found widely in the air, soil, groundwater, and drinking water. The levels of chromium in surface water and groundwater are typically influenced by regional geology, processes of mineral weathering, rates of sediment accumulation, and rainfall trends (Health Canada, 2016). Regions are characterized by mafic or ultramafic volcanic or metamorphic formations. , lacking quartz and rich in ferromagnesian minerals, may naturally have high chromium concentrations in groundwater, especially in ophiolite complexes and serpentine-rich units. Normally, chromium levels in uncontaminated water are very low, typically less than 1 µg/L. However, contamination of drinking water may occur due to leaching from landfills or

anthropogenic activities releasing chromium into the environment (World Health Organization, 2020).

Zinc can be found in both surface water and groundwater, permeating the surroundings via various sources such as Mine effluent, industrial and municipal discharges, and urban surface water runoff. The weathering of soil particles containing zinc also contributes to its presence in the environment (Noulas et al., 2018). As stated by the Food and Agriculture Organization (FAO) and the World Health Organization (WHO), water intended for consumption with zinc levels exceeding 3 mg/L may appear opalescent, form a greasy film when boiled, and have an unpleasant astringent taste (FAO/WHO, 1972). The zinc content in natural (unfertilized and uncontaminated) soil depends on factors like the chemical composition of the parent rock and the extent of weathering processes (Chesworth et al., 1991). In magmatic rocks, zinc concentrations typically range from 40 to 120 mg/kg, while in sedimentary rocks, they vary from 80 to 120 mg/kg in argillaceous sediments and shales and drop to 15–30 mg kg^{-1} in sandstones and in limestones and dolomites it is 10–25 mg kg^{-1} (Kabata et al., 2000).

The presence of iron in groundwater occurs naturally due to its presence in subterranean rock formations and the infiltration of water from precipitation through them. When the water percolates it dissolves some iron from the rocks and accumulates in aquifers, contributing to groundwater composition. 5% of the iron-containing underground rocks in the Earth, its occurrence is widespread across various geographical regions globally. Water containing iron typically manifests in three primary forms and is rarely detected at concentrations surpassing 10 mg l^{-1} or ppm (Ityel, D. (2011)). Iron (Fe) is abundant in the Earth's crust, primarily found in the form of ferromagnesian silicates, and it's also a significant element in certain soils (Jhon et al., 2010). The World Health Organization (WHO) and the Pakistan Council of Research in Water Resources (PCRWR) recommend a limit of 0.3 mg/L for iron (Fe (II)) in groundwater (PCRWR 2017) (WHO 2017)

Geologic factors such as the geology of the region, the type of rock, and the hydrological cycle can all impact the distribution and concentration of uranium and radon in drinking water sources. The concentration of these elements can also vary depending on the source of the water, the treatment processes used to purify the water,

and the distribution network used to transport the water to consumers (Tehseen., et al. 2019).

In this study, we will be able to identify the concentration of radon, chromium, zinc, and iron in the ground water sources of the area under study. Also, I will be able to produce a radon-prone map. We will try to fill the gaps and report geological and radioactive information. In the Karak district, both surface and groundwater resources are scarce, and their utilization and replenishment are crucial for sustainable development. In most parts of Karak, there's a decrease in the water table because of the excessive extraction of groundwater for domestic use and irrigation. The quality of water is also declining due to the overexploitation of groundwater.

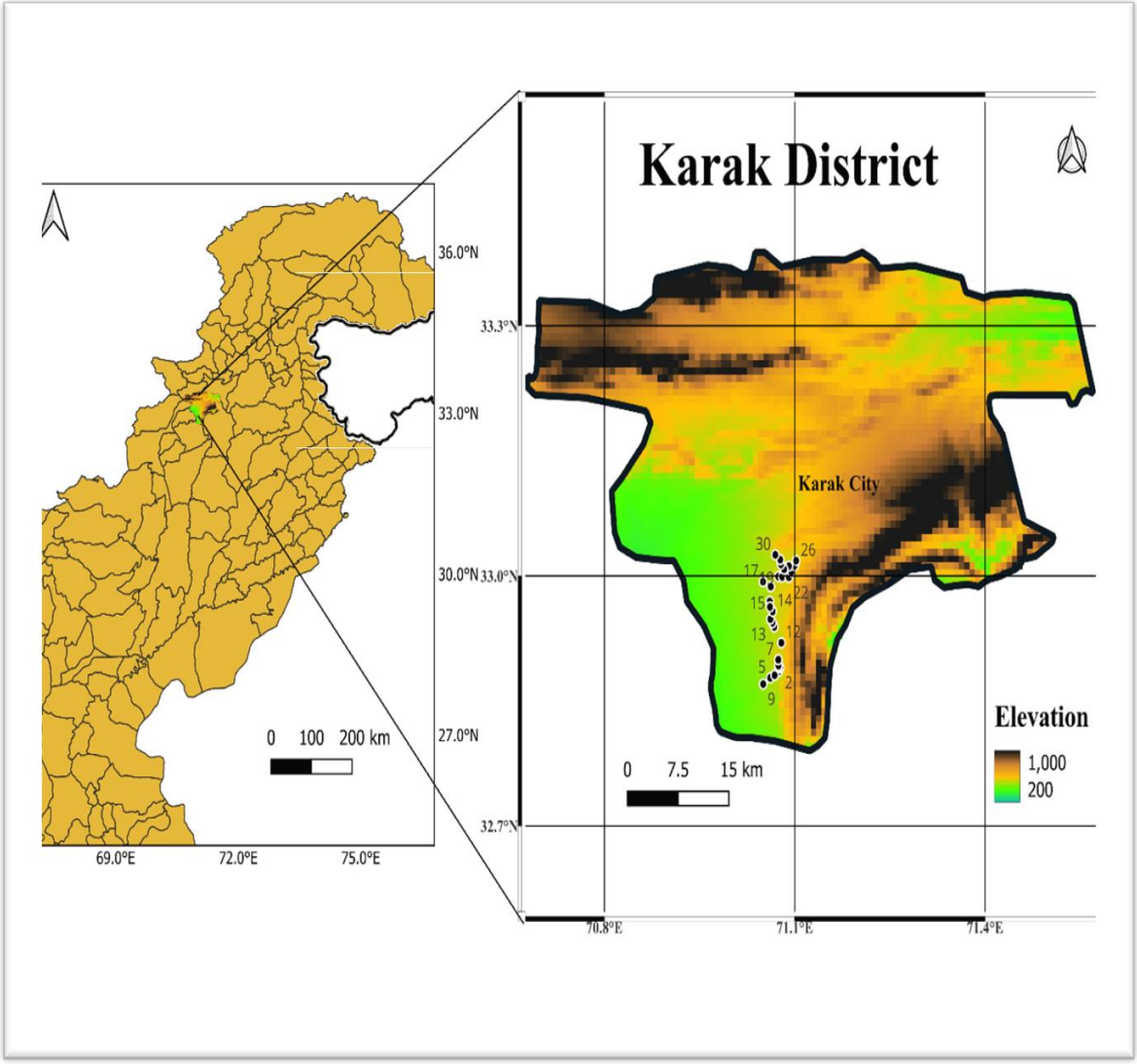

Figure 1: Map of the study area with sample location

2.2 Location And Accessibility

The area under study is the southern part of Karak city, situated in the northwestern part of the country Pakistan in the Khyber Pakhtunkhwa province which is easily accessible through Highways and motorways. The coordinates of the Karak region are (33.1277° N, 71.0973° E). The samples were collected from 30 different locations.

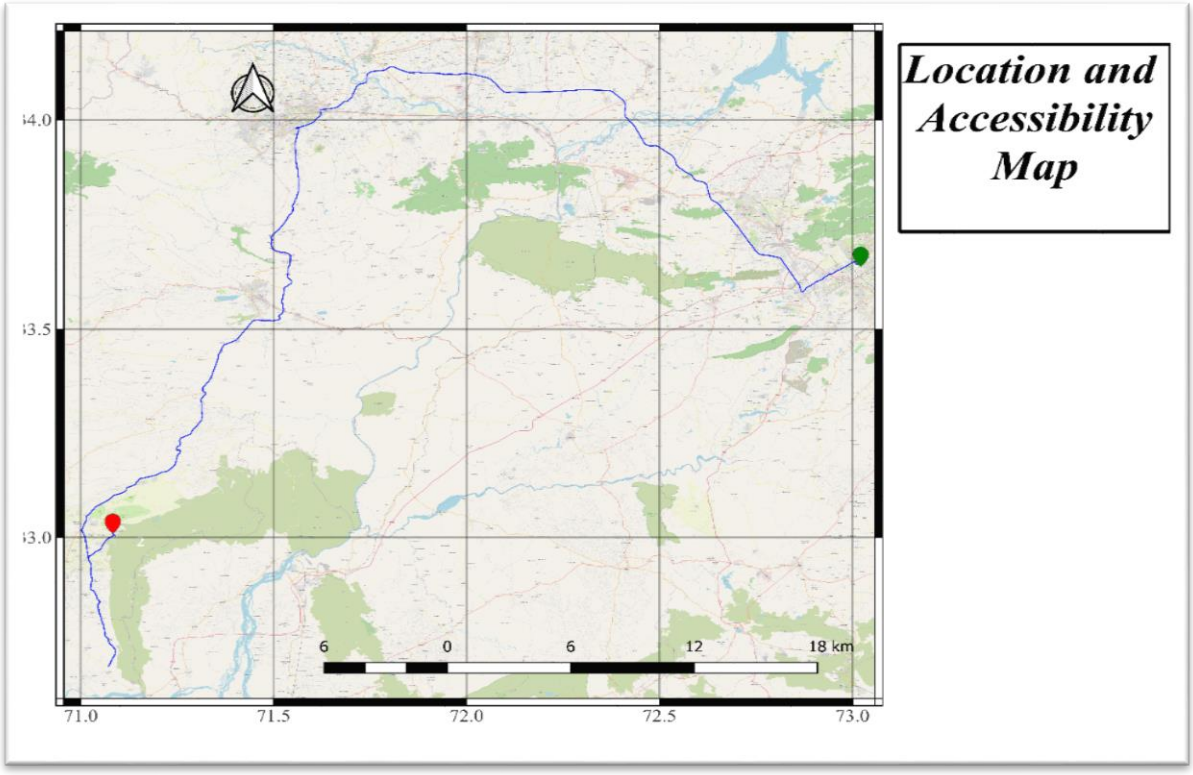

Figure 2: Location and Accessibility map

The following table presents the coordinates alongside the respective names of various locations. This comprehensive compilation serves as a valuable resource for accurately identifying geographical positions.

Table 1: Sample Location and Coordinates

SAMPLE NO.	LOCATION	CO-ORDINATES
1	Shnawa Gudikhel Tube well	32°53'08.0"N 71°04'29.0"E
2	Shnawa Gudikhel Tube well	32°53'24.0"N 71°04'38.0"E
3	Shnawa Gudikhel Pressure Pump	32°53'26.0"N 71°04'28.0"E
4	Shnawa Gudikhel Hand Pump	32°53'33.0"N

		71°04'28.0"E
5	Shnawa Gudikhel Hand Pump	32°52'40.0"N 71°03'41.0"E
6	Shnawa Gudikhel Pressure Pump	32°52'51.0"N 71°04'06.0"E
7	Shnawa Gudikhel Hand Pump	32°53'58.0"N 71°04'27.0"E
8	Shnawa Gudikhel Tube well	32°52'51.0"N 71°04'06.0"E
9	Shnawa Gudikhel Hand Pump	32°52'13.0"N 71°03'01.0"E
10	Shnawa Gudikhel Hand Pump	32°56'20.0"N 71°04'04.0"E
11	Shnawa Gudikhel Pressure Pump	32°56'38.0"N 71°03'54.0"E
12	Shaheedan Banda Hand Pump	32°55'11.0"N 71°04'44.0"E
13	Shaheedan Banda Tube Well	32°56'53.0"N 71°03'42.0"E
14	Shaheedan Banda Tube Well	32°57'27.0"N 71°03'55.0"E
15	Ganderi Khattak Hand Pump	32°58'10.0"N 71°03'38.0"E
16	Ganderi Khattak Tube Well	32°59'14.0"N 71°03'44.0"E
17	Ganderi Khattak Tube Well	32°59'35.0"N 71°04'00.0"E
18	Ganderi Khattak Pressure Pump	32°57'46.0"N 71°03'40.0"E
19	Takhti-e-Naserati Hand Pump	32°59'57.0"N 71°04'27.0"E
20	Takhti-e-Naserati Pressure Pump	32°59'56.0"N 71°04'49.0"E
21	Takhti-e-Naserati Pressure Pump	33°00'07.0"N 71°05'18.0"E
22	Takhti-e-Naserati Pressure Pump	32°59'54.0"N 71°05'27.0"E
23	Takhti-e-Naserati Hand Pump	33°00'18.0"N 71°05'41.0"E
24	Takhti-e-Naserati Hand Pump	33°00'45.0"N 71°06'00.0"E
25	Takhti-e-Naserati Hand Pump	33°00'42.0"N 71°05'27.0"E
26	Takhti-e-Naserati Hand Pump	33°01'06.0"N 71°06'08.0"E
27	Takhti-e-Naserati Pressure Pump	33°00'29.0"N 71°04'60.0"E
28	Takhti-e-Naserati Tube Well	33°00'50.0"N 71°04'42.0"E
29	Takhti-e-Naserati Tube Well	33°01'10.0"N 71°04'38.0"E
30	Takhti-e-Naserati Pressure Pump	33°01'31.0"N 71°04'10.0"E

2.3 Hydrogeology

The aquifer's estimated thickness varies from 10 to 30 meters and is generally confined or semi-confined. Within the northeastern section of the catchment area in the northwest., the groundwater quality is notably poor due to the rock salt present in the northern mountains. This salt dissolves with runoff water, leading to groundwater contamination through deep percolation. Groundwater flows under phreatic conditions within the weathered layer and fractured zones at deeper levels. The alluvial fill is highly heterogeneous, rich in silt and clay, and locally contains gravel and sand beds found in boreholes. The expulsion from open wells is measured at 0.0349 Mm3/year. In contrast, the average recharge of the alluvial aquifer annually, estimated to be approximately 2.7 Mm3/yr (equivalent to 3.0 cusec), matches the average annual discharge (Kruseman et al., 1988). The groundwater level ranges from 29.03 to 238.66 meters, indicating a vague groundwater divide that aligns with the surface water divide. Based on a survey conducted in 2001 by the Planning and Development Department of Khyber Pakhtunkhwa, supported financially by UNICEF, it was found that from a complete population of 19 million residents in this region, approximately 59% have the availability of clean and safe drinking water. This access is facilitated through various sources such as pipelines, open wells, enclosed wells, ponds, springs, rivers, and canals.

The Karak District, with an entire population exceeding 460,000 inhabitants, resides in a semi-arid region characterized by an average annual rainfall of merely 200 mm. Situated within the Khyber Pakhtunkhwa province, this area grapples with a dire shortage of drinking water, a challenge exacerbated by rapid population growth and widespread poverty. The district's focal point, Karak city, harbors over 34,000 residents and has long been plagued by inadequate access to clean water. Groundwater, prevalent throughout much of the region, is often saline, with only sporadic pockets of potable water available.

Despite efforts by the Khyber Pakhtunkhwa Public Health Engineering Department to install tube wells for piped water distribution, merely half of Karak city's population benefits from this system, and many tube wells are either dysfunctional or yield brackish water due to overuse. The water crisis extends beyond Karak city, impacting the entire district with equal severity. The declining groundwater levels observed in

Karak City and its neighbouring villages can be attributed to a significant disparity between the rate of discharge and recharge. Over the past four decades, the population explosion has led to the encroachment upon the seasonal streams, which historically served as vital sources for recharging the region's freshwater reservoirs. As these streams have been increasingly utilized for residential construction, the natural replenishment of groundwater has been severely hampered. Presently, the primary source of recharge stems from a perennially flowing stream originating from salt mines situated to the north of Karak city and its surrounding areas. However, the water from this source has acquired a brackish quality due to its saline nature, rendering it unsuitable for both drinking and agricultural purposes. Despite its unsuitability, the lack of viable alternatives compels residents to resort to using this brackish water for their daily needs, including drinking and household chores. Access to this brackish water is further compounded by its limited availability in close proximity to residential areas, necessitating the arduous task of fetching water from distant wells. In addition to tube wells, residents also rely on water from hand pumps, natural springs, and open wells to meet their daily water needs.

Water samples were systematically gathered from various sources including tube wells, pressure pumps, and hand pumps located to the south of Karak city. The objective was to assess the concentration of radon using the RAD7 electronic apparatus. This initiative aimed to determine whether the residents of the region face any potential health risks associated with radon exposure, alongside the existing pollutants found in drinking water as previously stated.

2.4 Aims And Objectives

The primary objective of this research is to review current studies on the investigation of radon, iron, chromium, and zinc levels in drinking water sources. Specifically, the research aims to:

a. To identify the concentration of Radon in drinking water sources.
b. To prepare a radon-prone map of the study area.
c. To identify the concentration of Heavy Metals (Fe, Cr, Zn) in drinking water sources.
d. To prepare a spatial interpolation map of the study area.

2.5 Literature Review

The geological landscape of Karak, as outlined by Ullah, Hussain, et al. (2013), showcases a diverse range of rock formations, encompassing the Nagri, Chinji, Dhok Pathan, and Soan formations. These formations contribute to the geological richness of the area, attracting scientific interest and exploration endeavors. Access to clean and safe drinking water is a fundamental human right, as emphasized by Tahir (2004) and Ilyas et al. (2017). However, the suitability of water for consumption depends on its quality, which encompasses both biological and physio-chemical properties, as highlighted by Rezaee et al. (2001).

Khan et al. (2022) have reported elevated concentrations of radon in the drinking water sources of Karak City. The presence of radon, originating from uranium decay in geological formations, poses health risks to the local population, as emphasized by Khan et al. (2011). Moreover, Khan et al. (2014) suggest that natural springs in the area also contain radon, contributing to potential health hazards. Radon has been detected in the drinking water sources of the Karak City reported by Khan et al., (2022) that unexpectedly high concentrations of radon (Rn) in soil may be observed, exceeding levels typically associated with uranium decay in the earth. Major migratory pathways for radon are predominantly formed by faults, cracks, and fractures in the bedrock. Several studies have demonstrated that abnormal concentrations of radon are more likely to occur along active faults compared to background levels (Khan et al., 2022). Increased radon gas concentrations near cliffs or steep slopes can be linked to several factors, including the migration of radon gas within fault zones or fluctuation in radon production influenced by shifts in the near-surface geological layers associated with faults. The findings of Khan et al., (2022) provide substantial indications of convective movement of 222Rn taking place in specific, localized spots along fault lines. Radon has a two-fold impact on human life. It serves as a valuable tool for detecting and forecasting seismic events, volcanic eruptions, fault activity, and hydrological research when present in soil, water, and rocks. Conversely, elevated radon levels in indoor settings and drinking water can pose a notable health hazard to people due to its cancer-causing properties. (Khan et al., 2011).

As per Khan et al. (2022), various rock and soil types act as sources of radon gas. Rock formations with a higher likelihood of radon emission include glauconitic

sandstones, carbonaceous shales, carbonate rocks (karst topography), fluvial deposits, chalk, tillites, phosphorites, bauxite, granites, certain coal deposits, metamorphosed rocks with granitic composition, graphite schists, silica-rich volcanic rocks, fractured or faulted rocks, and specific contact metamorphic rocks. Conversely, rock types such as non-organic shales and siltstones, quartzose sandstone, and silica-deficient igneous and metamorphic rocks tend to emit radon less frequently. It's worth noting that localized uranium deposits in hydrothermal vein deposits within igneous and metamorphic rocks, along with roll-front deposits in sedimentary rocks, can be exceptions and contribute to the emissions of radon.

Chromium, zinc, and iron are among the trace metals found in water sources, influenced by geological factors such as rock composition and weathering processes, as discussed by Health Canada (2016), Noulas et al. (2018), and Ityel (2011). These metals can impact water quality and pose risks to human health, necessitating monitoring and mitigation efforts. The presence of trace metals in water sources, including chromium, zinc, and iron, poses significant concerns for water quality and human health, as highlighted in the literature. Health Canada (2016) underscores the influence of regional geology and mineral weathering processes on chromium levels in surface water and groundwater. Similarly, Noulas et al. (2018) emphasize the diverse sources contributing to zinc contamination in both surface and groundwater, including industrial discharge and urban runoff.

In the context of the Karak district, where access to clean drinking water is crucial, the geological composition plays a pivotal role in the occurrence of these trace metals. The literature indicates that areas with specific geological formations, such as mafic or ultramafic volcanic rocks, may naturally exhibit higher concentrations of chromium and zinc in groundwater due to mineral weathering processes (Health Canada, 2016; Noulas et al., 2018).

Furthermore, iron, a common constituent of underground rock formations, contributes to the natural presence of this metal in groundwater (Ityel, 2011). The dissolution of iron from rock formations as water percolates through them from precipitation results in its accumulation in aquifers, potentially impacting water quality. Both the World Health Organization (WHO) and the Pakistan Council of Research in

Water Resources (PCRWR) have established guidelines for iron levels in groundwater to ensure its suitability for consumption (WHO, 2017; PCRWR, 2017).

Understanding the distribution and behavior of these trace metals in water sources is crucial for assessing water quality and implementing effective management strategies. The geological factors influencing their occurrence, including rock composition and weathering processes, underscore the interconnectedness between geology and water quality in the Karak district. By investigating the concentrations of these trace metals in drinking water sources, this study aims to contribute to a comprehensive understanding of water quality issues and promote sustainable water resource management in the region. Javed, Tehseen et al. (2019) emphasize the role of geological factors in influencing the distribution and concentration of uranium, radon, and other elements in drinking water sources. Understanding these factors is essential for assessing water quality and implementing sustainable management practices.

This study aims to identify the radon, chromium, zinc, and iron concentrations in the drinking water sources of Karak, as well as produce a radon-prone map. By addressing gaps in existing research and reporting geological and radioactive information, this study seeks to contribute to a better understanding of water quality issues in the region. In summary, the literature reviewed provides valuable insights into the geological and hydrological aspects of the Karak district, highlighting the significance of water quality assessment and management in addressing public health concerns and promoting sustainable development.

CHAPTER 2

GEOLOGY AND TECTONICS

2.3 Regional Geology

In terms of geology, Pakistan is located between the Eurasian and Indian plates, with the provinces of Sindh and Punjab on the Indian plate's northwestern side, and a portion of Khyber Pakhtunkhwa and Baluchistan on the Eurasian plate, which mostly consists of the Iran plateau, Central Asia, and the Middle East. The boundary known as the Indus Suture delineates the northern extent of the Indian Plate in relation to the Asian Plate. Meanwhile, the Kohistan Island arc, resulting from intra-oceanic subduction within the Neo-Tethys, serves as the boundary between the Indian and Karakoram plates. Subsequently, this island arc collided with the Karakoram block (Ullah et al., 2020a, b).

Within the Kohat quadrangle, the bedrock comprises sedimentary formations spanning a wide range of ages, from the Jurassic period to the Pliocene epoch. In the quadrangle's northeastern and northwestern extremities, one encounters rocks like slate, slaty shale, and sandstone, which date back to the Precambrian or early Paleozoic eras. Additionally, the region's southern border has isolated areas where Triassic and potentially Permian rock formations are observed. These formations exhibit geological similarities to those found in the southeast Salt Range region (Meissner Jr., Charles R., et al., 1974).

The sedimentary sequence in the quadrangle showcases a substantial stratigraphic thickness, measuring more than 20,000 feet from the base of the earliest exposed Jurassic rocks to the Pliocene-aged Nagri Formation. Although the Dhok Pathan Formation, also from the Pliocene era and overlying the Nagri Formation in a conformable manner, was not directly measured, it is estimated to have an exposed thickness exceeding 5,500 feet. It's worth noting that the entire sequence has experienced significant folding and faulting processes, leading to extensive structural deformation (Meissner Jr., Charles R., et al., 1974).

A significant southward deformation was seen in the Kohat plateau during the late Miocene period. The main boundary thrust (MBT) is to the north of the plateau thus it defines its boundary on the north side, which brings the older rocks from the Kohat Range from the Mesozoic era on top of the younger rocks of the Kohat plateau from the tertiary era. Moving south, the Bannu basin marks the boundary of the Kohat plateau, while the Surghar Range demarcates its southeastern boundary. Adding to this, the left lateral Kurram Fault brings Mesozoic rocks into juxtaposition with Tertiary rocks toward the western side (Khan et al., 2022)

Karak is situated within the larger expanse of the Kohat Basin, positioned in the western segment of the Himalayan Foreland Folds and Thrust Belt. This basin stretches approximately 40 miles (70 km) in width, with variations on its northern and southern sides. The Kohat Basin is distinctly confined by the Main Boundary Thrust (MBT) to the north and the Surghar Range to the south. Separating the Surghar Range from the Salt Range is the Kalabagh Strike-Slip Fault (KSSF) (Khan et al., 1986; Lillie et al., 1987; Jaume and Lillie, 1988). In the east, the Kohat Basin extends to the river Indus, which acts as a natural demarcation separating it from the Potwar Plateau. On the western side, the Kurram Fault is found, serving as a boundary between the extremely deformed Mesozoic rocks of regions like Samana, Darsamand, Thal, and North Waziristan Agency, and the Eocene to Miocene deposits within the Kohat Basin (Khan et al., 1986). The southern boundary of the basin is delineated by the Bannu Basin. Within the Kohat Basin, the MBT is responsible for carrying Mesozoic and more recent strata over the molasse sediments of the Siwalik Group (Ahmed, Noor, et al., 2023)

Generally, the rocks exhibit intricate deformations, resulting in overlapping folding, as well as recurring faulting and thrusting. The stratigraphic composition of the study region encompasses the Bahadur Khel Salt layer (composed of salt intercalated with shale) and the Jatta Gypsum formation (featuring clay intercalations and gypsum). These formations, dating back to the Eocene epoch, represent the oldest exposed rocks in this area. Above these, we find the Kuldana (recognized for its red clays) and the Kohat Formation (comprising limestone and shale), both from the Eocene age. Similarly, the comprehensive rock series of the Siwalik Group, which spans from the Miocene to Pleistocene ages, consists of the Kamlial Formation (including sandstone, siltstone, and conglomerate lenses), the Chinji Formation (comprising shale and

sandstone), the Nagri Formation (characterized by massive sandstone and shale), the Dhok Pathan Formation (featuring friable sandstone), and the Soan Formation (containing pebbles, sandstone, and shale). It's important to note that this series overlays the Eocene sequence within the region. The District of Karak is rich in substantial deposits of evaporites, hydrocarbons, coal, and uranium (Khan et al., (2022)).

The area is characterized by a substantial succession of molasse sediments that are part of the Siwalik Group. These sediments can be stratigraphically categorized into the Lower, Middle, and Upper Siwaliks. Collectively, the Siwalik group in this area includes shales, conglomerates, and sandstones. Notably, the region features the prominent KT, a major thrust fault oriented approximately east to west. Along this fault, gypsum beds dating back to the Eocene era have been thrust in a southward direction, overlying the Lower Siwalik shales and sandstones of the Miocene age. Additionally, a significant geological feature in the area is the Karak Anticline, which stretches in a roughly northeast-southwest direction. This anticline is situated in the Karak trough southern part, positioned on the southern side of the KT (Khan et al., 2014).

2.2 Geology of the Study Area

This district is subdivided into three Tehsils: Karak, Banda Daud Shah, and Takht-e-Nasrati. Geologically, Karak exhibits four distinct rock formations: Chinji formation characterized by reddish shale and sandstone, Nagri formation primarily composed of sandstone with intermittent shale layers, Dhok Pathan formation comprising sandstone, shale, and conglomerates, and Soan formation characterized by reddish-brown shale and greyish-brown sandstone. Within the study area uranium mineralization has been identified east of Takht-e-Nasrati extending to the Shanawa Gudi-Khel area, covering a north-south strip of approximately 19 kilometres. This mineralization manifests in the form of yellow-colored secondary uranium mineral carnotite (K2UO2)2(VO4).3H2O. Azizullah and Khan (1998) identified two distinct types of sandstone bodies within the Chinji Formation at the Takhti Nasrati-Shanawah section of the Shinghar-Surghar Range. These are categorized as follows:

A) Multistoreyed major sandstone bodies, with a minimum thickness of 3 meters, and each story measuring 3-5 meters thick.

B) Overbank fines, characterized by intercalated layers of sandstone and mudstone, primarily distributed in the lower segment of the formation.

The presence of diverse sedimentary structures indicates that the sandstone bodies were formed through deposition by paleochannels dominated by sand, accompanied by subordinate gravels. Conversely, the overbank fines are attributed to flood sediments deposited by a meandering river system. The geology of the study area is characterized by a diverse range of rock types and geological features. The region exhibits various sedimentary formations, including sandstone, shale, and conglomerates, indicating past depositional environments such as river systems, floodplains, and coastal plains. Tectonic activity has played a significant role in shaping the landscape, resulting in the uplift of mountain ranges and the formation of geological structures like folds and faults. Additionally, Takht-e-Nasrati may host mineral deposits, contributing to its geological diversity and potential economic significance. Overall, the geology of Takht-e-Nasrati reflects a complex history of geological processes and formations, providing valuable insights into the region's geological evolution (Kafayat 2009)

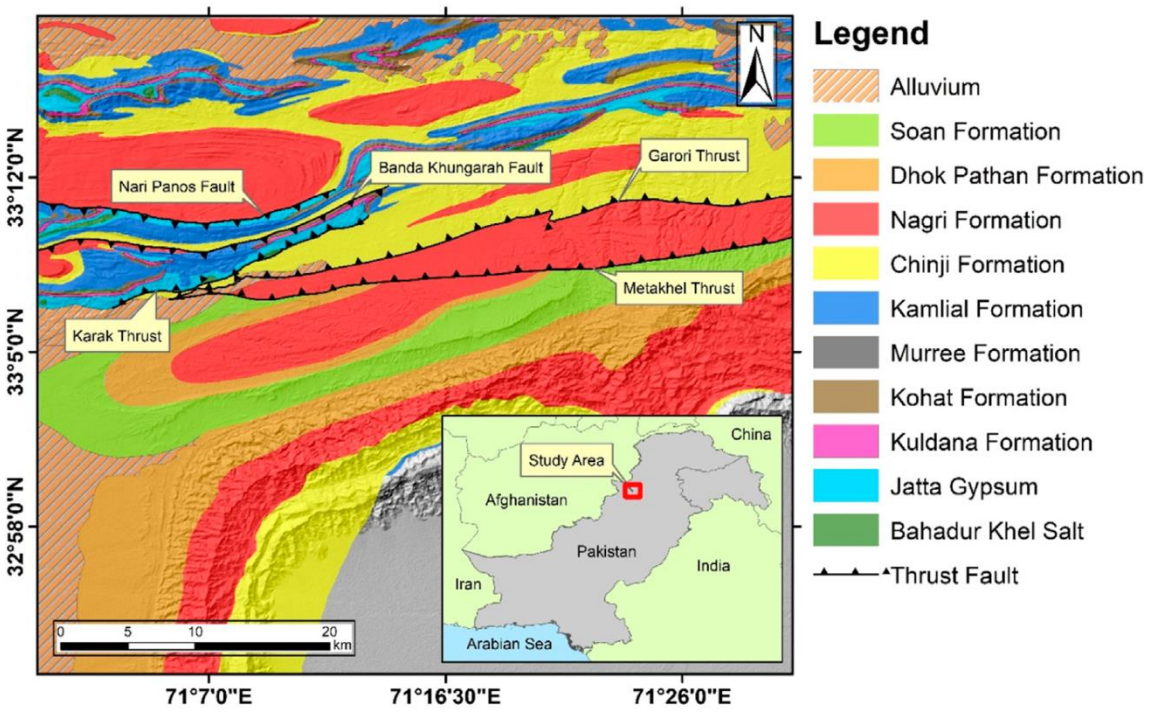

Figure 3: Geology of the study area (Khan et al., 2022)

2.3 Tectonic Setting

The magnificent Himalayan Mountain range, extending approximately 2500 km along the Indo-Pakistan plate margin, was formed by the forceful collision of the Indian Plate with the Eurasian Plate. Pakistan occupies the northwestern portion of the Indian Plate and the southeastern part of the Afghan-Helmand Plate (Ahmad, Sajjad, et al., 2017). The tectonic dynamics in Pakistan are influenced by both convergent and transform tectonics, particularly concerning the Afghan-Helmand block. This collision caused the Indian Plate to move northward at a rate ranging from 3 to 5 cm per year (Ahmad, Sajjad, et al., 2017).

As a consequence of this ongoing collision, the northern margin of the Indian Shield is being overridden by a series of south-verging thrusts. These thrust sheets, originating from the Himalayas, transport their erosion products into the actively migrating foredeep, which, in turn, is also moving southward. As part of this dynamic fold and thrust belt, the Kohat plateau exhibits a distinctive thrust sheet geometry, influenced in part by an Eocambrian evaporite sequence that functions as a basal decollement horizon (Jaume & Lillie, 1988).

Karak City serves as the administrative hub of this district within the region. Geographically, Kohat plateau occupies coordinates ranging from 70° to 74° E longitude and 32° to 34° N latitude, spanning an extensive area of approximately 10,000 square kilometers. This plateau represents the westernmost region of significant deformation within the Himalayan Foreland Fold Thrust Belt(Ullah et al., 2006).

Across the plateau's expanse, a prominent feature is the presence of a series of anticlines and synclines oriented roughly in an east-west direction. These geological formations have taken shape as a consequence of the ongoing collision between the Indian and Eurasian tectonic plates, offering captivating exposures of Cenozoic sedimentary rocks (Khan et al., 1986).

The Kohat plateau is surrounded by significant tectonic features, including the Surghar Range Thrust (SRT) in the south, the Main Boundary Thrust (MBT) in the north, the Kurram Fault in the west, and the Kalabagh Fault (running alongside the Indus River) in the east (Meissner et al., 1974; Jaume and Lillie, 1988). Notably, the

first comprehensive geological map of this plateau was officially published by the United States Geological Survey (Ahmad et al., 2005).

The Kohat plateau and Bannu basin constitute the northernmost segment of the Himalayan foreland basin, which some researchers have characterized as a foreland fold and thrust belt. Remarkably, it stands as the world's most extensive and active collision zone. This collision zone stretches from Myanmar (Burma) in the west, traversing northern India, Nepal, and southern Tibet, before reaching northern Pakistan. Within this vast region, the relentless collision between the Indian and Eurasian plates is driving substantial foreland thrusting on a continental scale.

The region is marked by significant tectonic disturbances, characterized by several prominent thrust faults, including the Karak Thrust, Banda Khungarah Fault, Garori Thrust, Methakhel Thrust, and Nari Panos Fault. The Jatta Gypsum layer is displaced over the Chinji Formation along the Karak thrust. Likewise, the Methakhel and Garori thrusts position the Nagri Formation above the Chinji Formation. Likewise, both the Banda Khungarah and Nari Panos faults act as back-thrust faults, bringing older Eocene rocks atop Pliocene-aged rocks within the area (Khan et al., 2022).

Karak fault, which dips toward the north, is situated precisely at the demarcation line between the Bannu Basin and the Kohat Plateau. Its orientation runs predominantly from east to west, displaying moderate dip angles. Functionally, it thrusts the rock layers of the Jatta Gypsum and Mami Khel Formation over the Chinji Formation in the southern direction. The Karak Fault is a noteworthy feature, representing the southernmost extension of exposed evaporite facies on the surface of the Kohat Plateau (Shimasaki, Akihiro et al., 2017). In the southern part of the Karak Trough, positioned on the southern side of the Karak Thrust, lies a prominent anticline with an approximate NE-SW orientation, known as the Karak Anticline.

The Karak Thrust, a relatively recent and active geological fault, is located on the northern side of the Karak Trough, which forms a part of the Karak Tehsil in the Karak District within the Province of Khyber Pakhtunkhwa. Geographically, the Karak Trough occupies the southern periphery of the Plateau of Kohat, spanning coordinates between 71.0222° E - 71.3881° E longitude and 33.0200° N - 33.1200° N latitude. Positioned south of the Karak Thrust, this trough is bordered by the Bannu Basin to the

west, the Shakardara hills to the east, and the Shinghar-Surghar ranges to the south. Covering approximately 80% of Tehsil Karak, it includes Karak City and neighbouring villages to its north, south, west, and east (Khan et al., 2016).

Within the Karak Trough, the geological formations primarily belong to the Siwalik Group, dating back to the Miocene epoch. These geological structures showcase mild folding configurations, primarily orienting in an east-west direction, accompanied by linked thrust faults (Ali et al., 2010). The Karak Thrust, in particular, stretches northeast-southwest and exhibits a geological fault dipping towards the north. It juxtaposes the newer sedimentary rocks of the Miocene era from the Siwalik Group to the southern region with the older formations of Bahadur Khel Salt and Jatta Gypsum, dating back to the Eocene epoch, situated to the north.

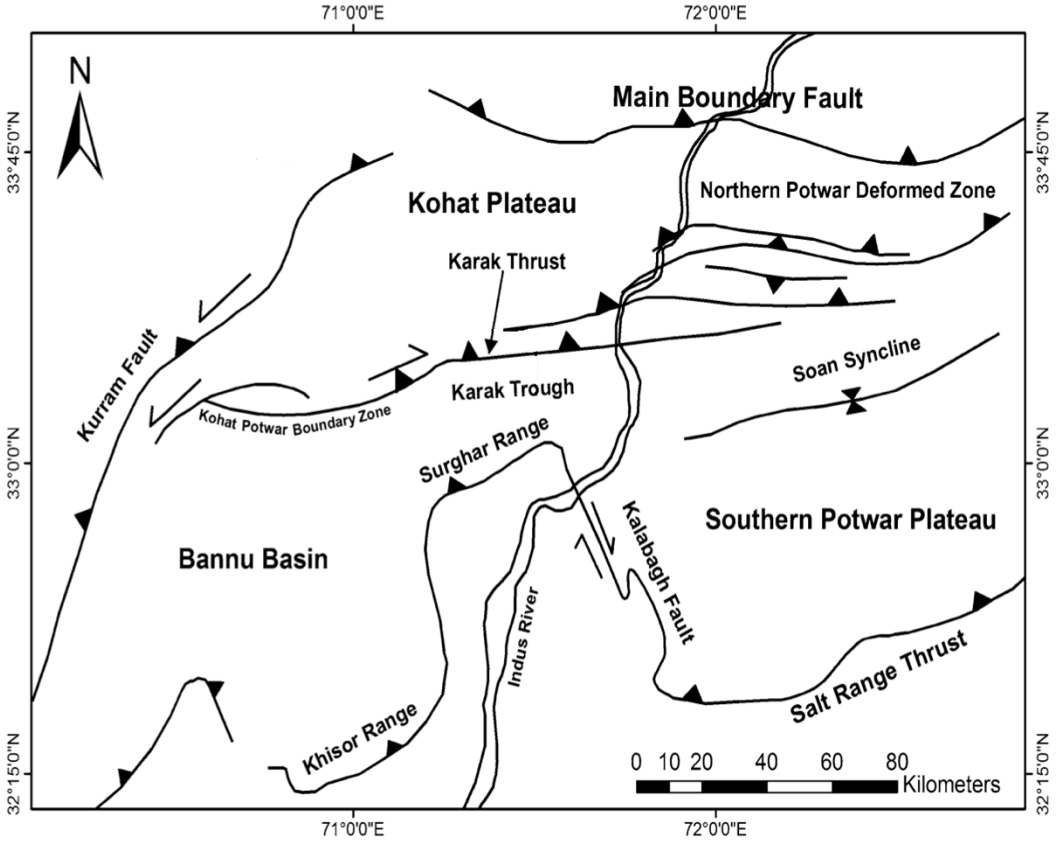

Figure 4: Tectonic Map of the Karak (Khan et al., 2022)

CHAPTER 3

STRATIGRAPHY

3.1 Stratigraphy

In the Karak area of the Kohat plateau, geological exposures from the Cenozoic era unveil a stratigraphic sequence characterized by Eocene evaporite and shelf sediments. Overlying this, there's a substantial molasse sequence that spans from the Late Oligocene to the Pliocene in terms of age.

The stratigraphic composition within the study region encompasses several key formations. These include the Bahadur Khel Salt layer, characterized by intercalated salt and shale, and the Jatta Gypsum formation, featuring intercalations of gypsum and clay. Remarkably, these formations trace their origins back to the Eocene epoch, making them the oldest exposed rock formations in this area.

Sitting above these formations, we encounter the Kuldana, notable for its distinctive red clays, and the Kohat Formation, which is predominantly composed of limestone and shale. These two formations also belong to the Eocene age. Additionally, the extensive rock series of the Siwalik Group, spanning from the Miocene to the Pleistocene ages, is comprised of several distinct units:

- The Soan Formation contains pebbles, sandstone, and shale.
- The Dhok Pathan Formation features friable sandstone.
- The Nagri Formation is recognized for its massive sandstone and shale layers.
- The Chinji Formation consists of shale and sandstone.
- The Kamlial Formation is characterized by sandstone, siltstone, and conglomerate lenses.

These formations collectively offer a rich geological record of the region

a. Bahadur Khel Salt

Initially designated as the "Kohat Saline Series" by Gee in 1945, this formation underwent a renaming process. Meissner et al. (1974) officially renamed it the "Bahaderkhel Salt" based on exposures observed in the Bahaderkhel salt quarry.

Bahaderkhel Salt is exposed in the north of Karak City, specifically in the Rahmatabad and Nari Panos areas. Its exposure typically occurs along thrust faults, where it serves as a relatively weak detachment level. Additionally, this salt formation can also be found in diapiric anticlinal cores. In terms of its characteristics, Bahaderkhel Salt is predominantly massive, occasionally displaying thin layers ranging from 5 to 15 centimetres in thickness. It exhibits a color spectrum from white to cream, occasionally featuring a subtle black hue. Clear halite crystals can also be found within this formation. Interestingly, in certain areas, it intermingles with intermittent clay and green shale layers, which are notable for their distinctive hydrocarbon odor (Fayaz Ali 1994).

The exact thickness of Bahaderkhel Salt remains uncertain due to its diapiric nature and the unexposed nature of its base. Nevertheless, according to Meissner et al. (1974), the thickness of Bahaderkhel Salt that is exposed thickness is approximately 100 meters. They have referred to it as the lateral facies' counterpart of the Panoba Shale, which can be observed in the northern section of the plateau (Fayaz Ali 1994).

While the lower contact of this formation remains hidden from view, the upper contact is conformable with the Jatta Gypsum. The age of the Formation is deduced to be Early Eocene, a conclusion drawn from the presence of well-preserved fossils, plant leaves, as well as bands of sandstone and clay that are interstratified with the rock salt layers. (Fayaz Ali 1994).

b. Jatta Gypsum

Jatta Gypsum was initially categorized as a component of Bahaderkhel Salt and was encompassed within Gee's (1945) "Kohat Saline Series." However, a reevaluation led to its renaming as "Jatta Gypsum." It is now regarded as the upper section of the "Kohat Saline Series," based on observations made at the Jatta Ismailkhel Gypsum quarries (Meissner et al., 1974).

The main constituents of the Jatta Gypsum Formation consist of gypsum, with occasional intercalations of gypsiferous shale and bentonitic clay. The gypsum itself varies in color from white to greenish white and gray, presenting a massive to thick-bedded structure. Notably, the outcrops of this Formation are characterized by distinct

gray and white bands with rugged, sharp edges. In certain areas, the gypsum takes on a darker hue, ranging from gray to black, owing to a hydrocarbon coating on fractured surfaces, which imparts a noticeable petroliferous odor. The clay layers within this formation exhibit colors spanning from greenish-gray to bluish-green and possess greasy and plastic characteristics. An estimated average thickness of approximately 50 meters is observed in the region. Within this geological context, Jatta Gypsum is considered to be the lateral facies equivalent of the Shekhan Limestone (Fayaz Ali 1994).

Structurally, numerous small-scale asymmetrical folds, varying in shape and size, have developed within the gypsum beds, largely attributed to processes such as thrusting, folding, and diapirism. In terms of stratigraphy, the Formation conforms smoothly above the Bahaderkhel Salt and underlies the Kuldana Formation. Although no fossils have been documented within the Jatta Gypsum, the presence of conformable contacts with the Eocene Formations both above and below provides strong evidence for assigning an Early Eocene age to this formation (Fayaz Ali 1994).

c. Kuldana Formation

The geological unit referred to as the "Kuldana Beds" was first coined by Wynne (1874). It was later referred to as the "Kuldana Series" by Middlemiss (1896) and identified as the "Mamikhel Clay" by Meissner et al. (1974). It was subsequently formally designated as the Kuldana Formation by Latif (1970).

This formation exhibits a thickness ranging from 50 to 60 meters, predominantly composed of clay, sandstone, and granule stone, particularly in its upper portion (as outlined by Wells, 1984). The clay within the formation displays hues of red to brownish-red and is characterized by its soft, gypsiferous, and calcareous nature. In the form of thin fibers and crystals, Gypsum is present. Meanwhile, the sandstone layers are reddish-brown, thinly bedded, and characterized by their hard, medium to coarse-grained texture, often displaying cross-bedding (Fayaz Ali 1994).

The Kuldana Formation originates from continental fluvial processes and was deposited by swiftly flowing streams within a semi-arid basin, marking the conclusion of a marine regression (as noted by Wells, 1984). Stratigraphically, the formation

maintains conformable lower and upper contacts with the Jatta Gypsum and Kohat Formation, respectively. The fossil assemblages discovered within this formation suggest an Early to Middle Eocene age (Fayaz Ali 1994).

d. Kohat Formation

The geological unit previously referred to as the Kohat Shale in Eames' work (1952) and the Kohat Limestone as identified by Meissner et al. (1974) was officially renamed the Kohat Formation by the Stratigraphic Committee of Pakistan in 1977.

In the lower section of the Formation, shale predominates in terms of lithology, presenting itself in shades ranging from greenish-gray to gray. These shale layers are thin-bedded, soft, calcareous, and notably rich in fossils. In contrast, the upper part of the Formation is characterized by fine-grained limestone, featuring thin to medium bedded structures, jointing, and an abundance of nummulites (Fayaz Ali 1994).

Stratigraphically, the Formation lies conformably over the Kuldana Formation, with a well-defined and sharp contact. However, the upper contact displays unconformity with the Kamlial Formation of the Rawalpindi Group. At this boundary, there is typically a thin conglomerate bed containing pebbles composed of limestone originating from the Kohat Formation, embedded within a sandy matrix. This unconformity between the Kohat and Kamlial Formations signifies a period of non-deposition during the Late Eocene to Oligocene era, preceding the onset of molasse sedimentation (Fayaz Ali 1994).

3.2 Molasse sedimentation

Molasse sedimentation within the Kohat-Potwar foreland basin commenced during the Late Oligocene or Early Miocene period. In the Karak region, these molasse sediments exhibit a distinctive characteristic known as the coarsening of grain size upwards. The geological sequence can be effectively divided into two main groups:

A. Rawalpindi Group
B. Siwalik Group

A. Rawalpindi Group

The term "Rawalpindi Group" was originally introduced by Pinfold in 1918 and subsequently endorsed by the Stratigraphic Committee of Pakistan in 1977. This geological group is attributed to the Miocene epoch and comprises two distinct rock units, namely the Murree Formation and the Kamlial Formation. However, it's important to note that in the study area, only the Kamlial Formation is visibly exposed.

i. Kamlial Formation

Lewis (1937) proposed the renaming of the Kamlial Stage originally identified by Pinfold (1918) to the Kamlial Formation, a nomenclature later endorsed by the Stratigraphic Committee of Pakistan in 1977. This geological formation is primarily characterized by its composition, which predominantly consists of sandstone with occasional lenses of conglomerate, accompanied by lesser amounts of siltstone and shale.

Within this formation, approximately 90% of its composition is comprised of grey to greenish-grey sandstone, which is notably thick-bedded, medium to coarse-grained, cross-bedded, and includes conglomerate lenses. Additionally, clay is present as soft thin interbeds within the sandstone. At the same time, the siltstone, which appears reddish-brown, is hard, fine-grained, thin-bedded, and interspersed with clay.

Fossils of vertebrates have been discovered within this formation, providing evidence of its Middle Miocene age (Pascoe, 1963). The Kamlial Formation features an unconformable lower contact with the Kohat Formation and a conformable upper contact with the Chinji Formation of the Siwalik Group (Fayaz Ali 1994).

B. Siwalik Group

The term "Siwalik" was initially introduced by Medlicott (1864) after the Siwalik Hills in India. Pilgrim (1913) later proposed a threefold classification of the

Siwalik System, encompassing the Lower Siwalik (comprising the Kamlial and Chinji zones), Middle Siwalik (encompassing the Nagri and Dhok Pathan Zone), and Upper Siwalik (including the Tatrot, Pinjor, and Boulder Conglomerate Zone).

Cotter (1933) proposed the consolidation of the Kamlial Stage with the Murree Formation, as the demarcation between these two entities was regarded as somewhat arbitrary. This proposal was endorsed by the Stratigraphy Committee of Pakistan. Ultimately, the Stratigraphy Committee of Pakistan replaced the term "Siwalik System" with the "Siwalik Group," comprising the following formations:

i. Chinji Formation
ii. Nagri Formation
iii. Dhok Pathan Formation
iv. Soan Formation

A coarsening upward molasse sequence is seen in the Siwalik Group in the Indo-Pakistan Subcontinent and boasts a considerable thickness, spanning several thousand meters. It has also yielded a wealth of vertebrate fauna (Pilgrim, 1913; Pascoe, 1963), which indicates its age as ranging from the Middle Miocene to the Early Pleistocene.

i. Chinji Formation

Lewis (1937) designated the term "Chinji Formation" for the "Chinji Stage" initially introduced by Pilgrim (1913). The Chinji Formation primarily outcrops along algads, local designations for dry stream valleys, and within the cores of synclines. Due to its relatively softer nature compared to the formations above and below, it often experiences compression, folding, and erosion, leading to the formation of narrow gullies.

The Formation predominantly consists of sandstone interlayered with clay and siltstone. Thin intraformational conglomerate lenses are also frequently observed. The sandstone exhibits shades of grey to brownish grey, is relatively soft, and displays crossbedding with a medium grain size. The silty clay appears in tones of brown, red to greyish-red and possesses a nodular texture. Siltstone

layers, brownish grey in color, interbed with laminated silty clay. The Chinji Formation has a well-defined and conformable lower contact with the underlying Kamlial Formation, and its upper contact with the overlying Nagri Formation is also distinct and conformable. Rich assemblages of vertebrate fossils (Pascoe, 1963) within the Chinji Formation suggest a Middle Miocene age.

ii. Nagri Formation

Lewis (1937) introduced the name "Nagri Formation" for the "Nagri Stage" originally described by Pilgrim (1913). Comprising primarily sandstone interbedded with clay, the Formation also incorporates intraformational conglomerate layers at various intervals.

The sandstone presents itself in a greenish-grey hue, with a medium to coarse grain size. It exhibits characteristics of cross-lamination, a massive to thick bedding structure, and well-defined joints. The clay component of the Formation is silty and varies in color from chocolate brown to reddish brown, occasionally containing siltstone interbeds.

The Nagri Formation's thickness at the Totaki section measures an astounding 4225 meters (Meissner et al., 1968), significantly greater than in other sections. A meticulous examination was conducted to determine whether this unusual thickness resulted from folding or faulting repetitions, but no evidence supporting such phenomena was discovered.

The Formation maintains a conformable lower contact with the Chinji Formation and is transitionally overlain by the Dhok Pathan Formation.

iii. Dhok Pathan Formation

Lewis (1937) opted to rename the "Dhok Pathan Stage" originally identified by Pilgrim (1913) as the "Dhok Pathan Formation." This name adjustment, deemed more suitable, was officially adopted by the Stratigraphic Committee of Pakistan in 1977.

The Formation attains a thickness of approximately 1000 meters and is primarily comprised of sandstone with clay interbeds. In the upper part of the Formation, conglomerates in the form of lenses and layers constitute significant components. The sandstone exhibits shades of grey to greenish grey, characterized as soft, coarse-grained, calcareous, thick-bedded, and cross-laminated. The clay within the Formation takes on hues of orange-brown or reddish-brown and is calcareous and sandy.

Notably, conglomerates found in the Dhok Pathan Formation consist of rounded to subrounded pebbles originating from igneous and sedimentary rocks. These conglomerates are poorly sorted and cemented within the loose sand and silty clay matrix. The Dhok Pathan Formation is distinguished by its remarkably rich vertebrate fauna assemblage within the Kohat Potwar Province (Pascoe, 1963). These fossils collectively suggest an Early to Middle Pliocene age for this Formation.

The Formation maintains a conformable lower contact with the underlying Nagri Formation. In contrast, the upper contact with the Soan Formation is disconformable.

iv. Soan Formation

The "Tatrot" and "Pinjor" Stages, initially identified by Pilgrim (1913), were officially designated as the Soan Formation by the Stratigraphic Committee of Pakistan based on the recommendation of Kravtchenko (1964).

Soan Formation stands out for its relatively larger conglomerate component compared to other formations within the area of investigation. This Formation is primarily characterized by a sequence of conglomerates, sandstones, and clays. The lower section is marked by greenish-grey sandstone, and reddish-brown clay, interspersed with conglomerates and lenses. The upper part comprises conglomerates cemented in a soft sandy matrix. These conglomerates are thick bedded, loosely compacted, and exhibit poor sorting. They consist of pebbles and cobbles derived from a range of rock types,

including gneiss, volcanic rocks, quartzite, and various other metamorphic and sedimentary rock fragments.

The thickness of the Soan Formation varies from 200 to 450 meters. It is separated from the Dhok Pathan Formation by a disconformity, with a reworked volcanic boulder bed at the base.

Table 2: Stratigraphic Column of Karak (Fayaz Ali 1994)

Age		Stratigraphy	Thickness in Study Area (m)	Lithology
Pliocene	**Siwalik Group**	Soan Formation	250 - 400	Conglomerate, Sandstone, and Clays
Miocene		Dhok Pathan Formation	1000	Sandstone with clay interbedding
		Nagri Formation	3000	Sandstone and Shale
		Chingi Formation	1000	Shale, Siltstone and Sandstone
	Rawalpindi Group	Kamlial Formation	550 - 600	Sandstone
Oligocene		Unconformity		
Eocene		Kohat Formaiton	1 - 6	Shale
		Kuldana Formation	50 - 60	Clay
		Jatta Gypsum	50 - 60	Gypsum
		BahadurKhel Salt	100	Salt

CHAPTER 4

METHODS AND METHODOLOGY

4.1 Methods

The fieldwork was meticulously conducted in the picturesque and geographically diverse Karak district of Khyber Pakhtunkhwa, known for its rugged terrain and rich cultural heritage. A comprehensive sampling effort targeted various locales within the Takht-I-Naserati and Shnawa GudiKhel areas of district Karak, each selected to represent a distinct environmental context. The assessment of radon concentrations in water samples gathered from various sites to the south of Karak city required the application of the RAD7 radon-in-air device. This instrument utilizes the RAD H2O technique, allowing for direct measurement of radon concentration within water samples. Integrated with predefined and standardized protocols, including a closed-loop aeration system, the RAD7 ensures consistent water and air volumes during analysis, eliminating potential variations due to flow rate fluctuations. Additionally, to assess heavy metal concentrations in the water samples, an atomic absorption spectrophotometer polarized Zeeman (Hitachi Model Z-2000) was employed. This sophisticated instrument enables precise measurement of heavy metal concentrations, including chromium (Cr), iron (Fe), and zinc (Zn), with high sensitivity and accuracy. Throughout the analysis process, stringent quality control measures were implemented, with water samples analyzed alongside standard solutions and repeat samples frequently assessed to verify the reliability and consistency of the acquired data. This comprehensive approach aims to provide thorough insights into radon activities and heavy metal contamination in the water sources of the Karak district, crucial for understanding potential health risks and informing remediation strategies.

4.2 Sample collection

In total, 30 samples were meticulously collected from different locations within these areas, ensuring a representative snapshot of the environmental conditions prevalent across the district. Each sampling site was carefully identified and documented, with precise coordinates recorded using a GPS application on a mobile device, guaranteeing accurate spatial data for subsequent analysis and interpretation.

To maintain the integrity of the samples and prevent any potential contamination, 250ml distilled plastic bottles were employed for collection. These containers were tightly sealed upon collection to preserve the original composition of the samples and minimize any external influences during transportation and storage. The rigorous attention to detail and adherence to best practices throughout the sampling process underscores the commitment to obtaining reliable and scientifically sound data, essential for the successful execution of subsequent analyses and the formulation of informed conclusions regarding the environmental dynamics within the Karak district.

Fig 5: Water Samples collection from a hand pump 250ml bottle was used.

4.3 Radon Measurement

In meticulous adherence to standardized scientific procedures, an exhaustive field expedition was undertaken to procure water samples for radon analysis, a radioactive gas of significant environmental concern. A total of 30 water samples, each measuring 250 ml in volume, were meticulously collected from diverse locations spanning the study area. This comprehensive sampling strategy ensured a representative selection of environmental conditions and geographic diversity crucial for robust analysis.

Each water sample was meticulously labeled, and the precise geographic coordinates of their collection points were methodically recorded in the field notebook. This detailed documentation facilitated accurate spatial referencing, ensuring the traceability and integrity of the sampling process. To maintain the integrity and fidelity of the collected samples, specialized 250 ml bottles were employed as containment vessels. These vessels were hermetically sealed upon collection, effectively safeguarding the samples from potential environmental contaminants during transportation and storage. Stringent precautions were observed during sample handling to minimize the risk of inadvertent alterations or the introduction of contaminants. Such meticulous care was imperative to preserve the original chemical composition of the samples and uphold the integrity of subsequent analyses

Upon completion of the field collection phase, the samples were expeditiously transported to the well-equipped facilities of Peshawar University for further processing and comprehensive radon analysis. Upon arrival, stringent protocols were followed to ensure the preservation and integrity of the samples prior to analysis. The samples were carefully stored under controlled conditions to prevent any degradation or alteration of their chemical composition, thereby safeguarding the accuracy and reliability of subsequent analytical results. This rigorous and methodical approach to sample collection and handling underscores our unwavering commitment to scientific rigor and underscores the importance of meticulous fieldwork in environmental research. Such meticulous documentation and adherence to standardized procedures are paramount in ensuring the validity and robustness of scientific findings, thereby facilitating informed decision-making and contributing to the advancement of knowledge in the field.

Radon measurements can be conducted either in the field, with on-the-spot readings, or by taking samples for analysis in controlled laboratory environments, where the impact of background radiation can be minimized through techniques such as shielding with materials like lead. Continuous and time-integrated measurements are typically carried out directly at the measurement site, while instantaneous measurements can be performed either on-site or within a laboratory setting. To evaluate Radon concentrations in water samples obtained from multiple locations in the south of Karak city, the RAD7, which is a radon-in-air monitor, was utilized for the measurement of radon activities in the National Center of Excellence in Geology Peshawar. This determination was carried out utilizing the RAD H2O technique, which leverages predefined and standardized protocols integrated into the RAD7 instrument. These protocols enable a straight assessment of radon levels within the samples of water itself. The methodology relies on a Closed-circuit aeration system, ensuring that both the water and air volume remain persistent and are not contingent on flow rate variations (Khan et al., (2014)).

Great care was exercised in the collection of water samples to ensure they remained entirely unexposed to open air. The RAD7 instrument offers users a choice between two distinct protocols, namely Wat 250 and Wat 40, Enabling them to quantity radon levels in two containers of varying capacities (250 or 40 ml) that are included with the apparatus. For my study, plastic bottles with a capacity of 250 ml were used. Each time a sample was analyzed to measure its radon concentration, the appropriate protocol was selected within the instrument's setup. While performing the experiments, a bottle containing the water sample was linked to the RAD7, and then the incorporated inner air pump in the radon monitor was used to create a closed-loop air circulation within the water sample. This procedure enabled the removal of dissolved radon from the water sample and its transfer into the closed-air circulation. The continuous circulation of air through the water was maintained to extract dissolved radon until the RAD H2O system reached a state of balance, which usually took about 5 minutes. Once this equilibrium was achieved, no additional radon could be transferred from the water into the air loop (Khan et al., 2014).

In the predefined Wat 250 protocol for water analysis, the entire process typically takes 30 minutes to complete. At the beginning of the experiment, the RAD7's built-in

pump activates automatically for a 5-minute interval. In the process, it oxygenates the sample and conveys the radon that has been removed from the sample into the air located inside the measurement chamber of the RAD7 unit. Notably, over 94% of the original radon content in the water is degassed and transferred into the air loop during this 5-minute aeration stage. After precisely 5 minutes, the pump repeatedly stops, and the system enters a waiting period of an additional 5 minutes. Subsequently, the system commences counting. Another 5 minutes later, a concise explanation for a 5-minute cycle is printed. This process repeats once more 5 minutes subsequently and continues for two additional 5-minute periods. Upon completion of the run, which is approximately half an hour after initiation, the RAD7's connected printer produces a summary. This summary comprises the average concentration of the radon observed across four measured cycles, each lasting 5 minutes. It also exhibits a bar chart illustrating these four measurements along with an accumulated range. The radon absorption indicated in the summary is automatically measured by the RAD7 and pertains to the water sample (Khan et al., (2014)).

In situations where you can't analyze water samples immediately and need to wait for 24 hours before measuring, you have to correct the results for the natural decay of radon. This correction is done using a Decay Correction Factor (DCF), which can be computed using this equation.

$DCF = e^{(0.00755T)}$ (Equation 1)

In this equation:

- T represents the decay time in hours.
- 0.00755 is a constant representing the reciprocal (1/mean) life of a radon atom (specifically, 222Rn). The mean life of 222Rn is 132.4 hours.

So, you use this formula to calculate the DCF based on how long you've waited to measure the radon in the water sample. This correction factor helps adjust the results for the natural decay of radon over time (Khan et al., (2014)).

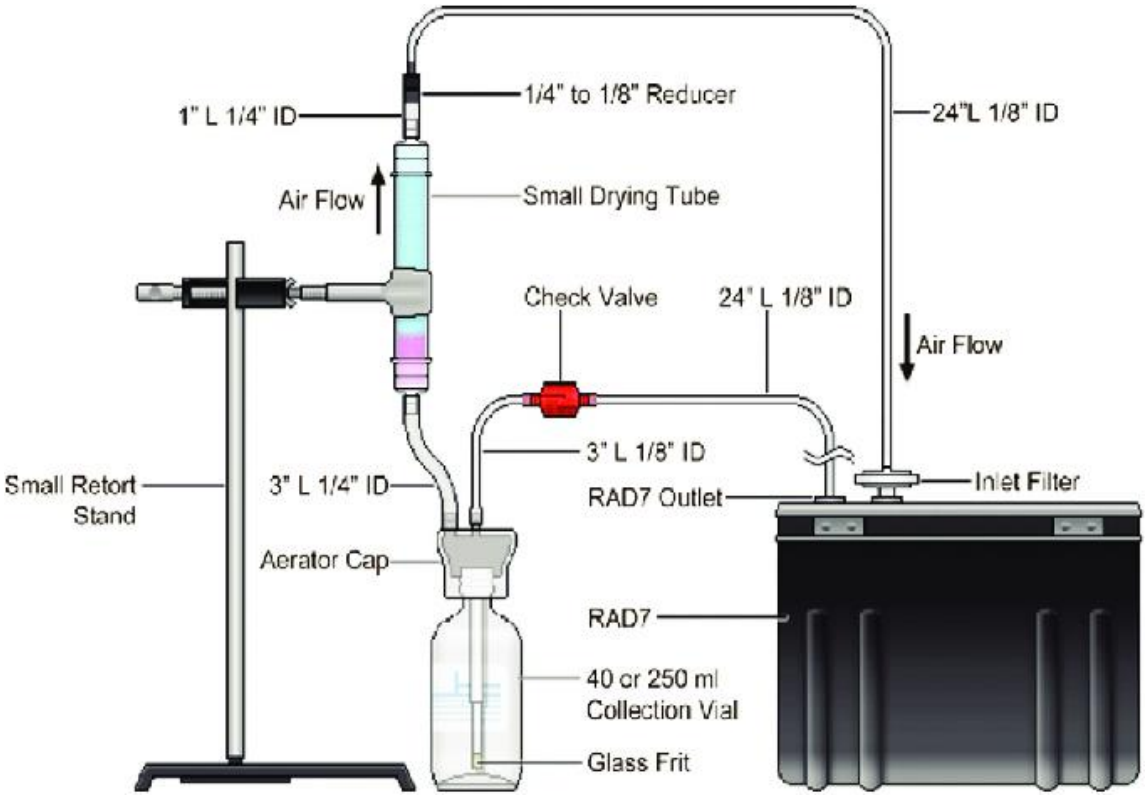

Figure 6: RAD7 set up for measuring 222 Rn water samples (Durridge Company RADH2O Manual, 2015).

4.4 Mean Radon Evaluation

The exposure to the radiation stemming from drinking water due to the presence of radon can be categorized into 2 separate components: (a) the dose resulting from radon ingestion and (b) the dose originating from radon inhalation. When radon and its progeny are ingested through drinking water, they primarily affect the stomach, contributing to the radiation dose. Nevertheless, radon gas dissolved in the water samples can also be transported to the indoor air during activities such as showering, thereby presenting a notable hazard of lung cancer through inhalation. Waterborne radon is considered a greater threat to public health compared to other water contaminants (Vitz E (1991)). The yearly mean effectual doses for both the inhalation and ingestion of the presence of radon in water were calculated utilizing the parameters specified in the 2000 UNSCEAR report.

$$EWIg\ (mSv\ a^{-1}) = CRnW \times C \times EDC$$

EWIg represents the ingestion effective dose, *CRnW* stands for the radon in water abundance (measured in kBq m^{-3} or Bq L^{-1}), and C represents the weighted approximation of water intake. (60 L a^{-1}), and *EDC* denotes the coefficient for effective dose in ingestion (measured in 3.5 nSv Bq^{-1}).

$$E_{WIh}\ (mSv\ a^{-1}) = C_{RnW}\ x\ R\ x\ F\ x\ O\ x\ DCF$$

E_{WIh} represents the effective dose for inhalation, R denotes the ratio of radon in air to the radon in water (measured in 10^{-4}), F represents the equilibrium factor between radon and its progenies (measured as 0.4), O signifies the average indoor occupancy time per individual (7000 ha^{-1}), and DCF stands for the dose conversion factor for radon exposure, which is 9 nSv/(Bq h m^{-3}).

4.5 Radon Measurement Technique

When a radon (222Rn) atom emits an alpha particle, a 218Po ion is generated which is positively charged, generated within the RAD7 compartment. Within the chamber, there is a sturdy electric field that guides the 218Po ion toward a silicon alpha detector, where it becomes affixed. Subsequently, an alpha particle is emitted during the decay of the short-lived 218Po nucleus, occurring on the surface of the detector.

There exists a 50% possibility that the alpha particle will penetrate the detector and generate an electrical signal. The magnitude of this signal is directly linked to the energy of the alpha particle. Distinct polonium isotopes emit alpha particles with diverse energies, leading to signals of varying intensities in the detector. These signals are documented in distinct energy ranges (Khan et al., 2014).

When conducting a water sample analysis with the Wat 250 protocol in sniff mode, the RAD7 device calculates the average radon concentration after approximately 30 minutes, relying exclusively on the 218Po activity. Unlike certain other methods, it doesn't wait for the radon in the air loop to reach balance with its progenies before making this calculation.

What sets RAD7 apart is its exclusive utilization of alpha particles emitted by 218Po in sniff mode to measure the concentration of 222Rn. It disregards alpha particles

released by 214Po and other decay byproducts from prior analyses. This approach allows for multiple radon concentration analyses to be performed quickly (Khan et al., (2014)).

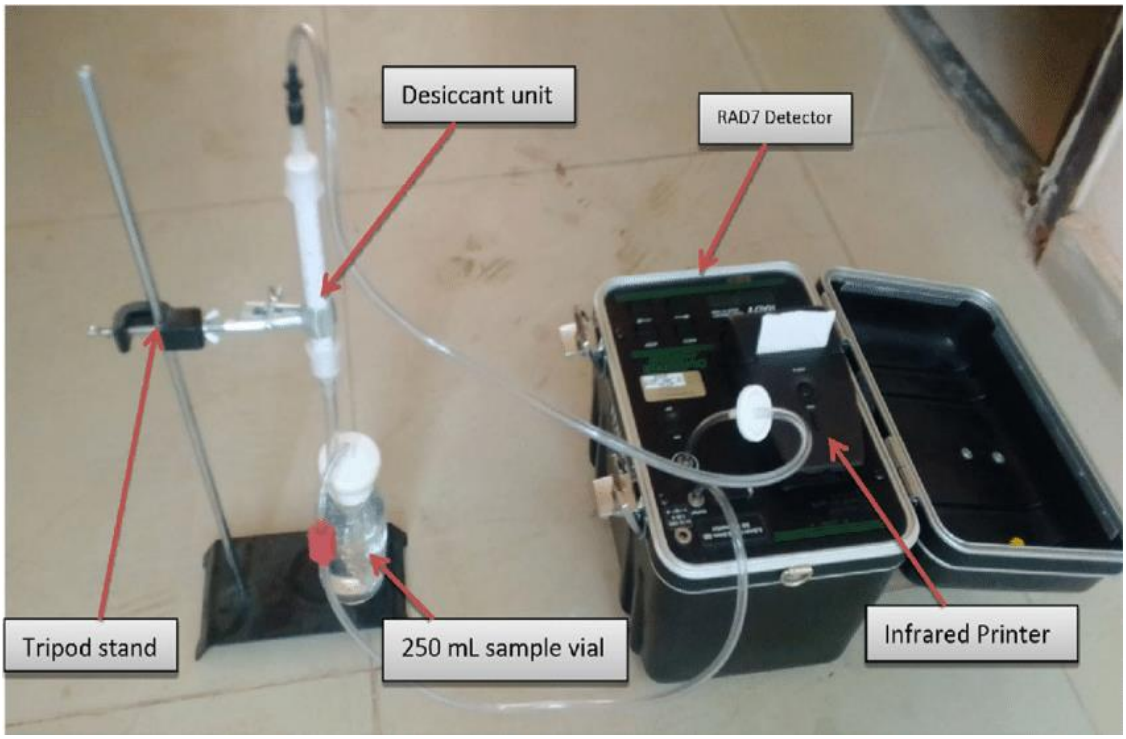

Figure 7: Experimental setup of RAD7 detector with RAD-H20 accessories used in this study.

4.6 Heavy Metals Measurements

The levels of heavy metals (chromium, iron, and zinc) were assessed by employing an atomic absorption spectrophotometer which is a Hitachi Model Z-2000. Rigorous analysis of water samples was conducted alongside standard solutions to uphold data quality. Furthermore, repeat samples were regularly scrutinized to evaluate the consistency and dependability of the obtained data.

Following rigorous scientific protocol, a comprehensive field sampling campaign was conducted in the study area to procure representative water samples for the analysis of heavy metals, specifically Chromium (Cr), Iron (Fe), and Zinc (Zn). A total of 30 samples were meticulously collected from diverse locations within the study area, ensuring spatial coverage and a robust representation of environmental conditions. Each sample was meticulously labelled, and relative coordinates were meticulously

documented in a field notebook to facilitate precise spatial referencing and subsequent analysis.

To maintain the integrity and quality of the collected samples, specialized 250 ml bottles were utilized for their containment. These containers were tightly sealed upon collection, meticulously safeguarding the samples from potential environmental contaminants during transportation and storage. Emphasis was placed on handling the samples with utmost care to mitigate the risk of unintended alterations or the introduction of contaminants.

After the field collection phase, the samples were transported to the esteemed facilities of Peshawar University for further processing and comprehensive testing. Upon arrival, stringent protocols were adhered to ensure the preservation and integrity of the samples before analysis. The samples were stored under controlled conditions to prevent any degradation or alteration of their chemical composition, thereby safeguarding the accuracy and reliability of subsequent analytical results.

This meticulous approach to sample collection and handling underscores our commitment to scientific rigor and ensures the validity and robustness of the data obtained. Such protocols must be rigorously followed to uphold the integrity of environmental research and facilitate informed decision-making processes.

Figure 8: Hitachi Model Z-2000 atomic absorption spectrophotometer (Adler et al., 2019).

4.7 Atomic Absorption Spectrophotometer Procedure

In the comprehensive procedure for analyzing water samples from Karak, KPK, utilizing the Hitachi Model Z-2000 atomic absorption spectrophotometer, meticulous steps are followed to ensure accurate and reliable results. Initially, each 250 ml water sample is meticulously labeled and, if necessary, filtered to eliminate any suspended particles. The samples are then acidified with nitric acid to stabilize metals and prevent precipitation, with optional digestion performed for complete dissolution of metals bound within organic matter. Following sample preparation, the atomic absorption spectrophotometer is primed for analysis in polarized Zeeman mode, optimizing sensitivity and precision. Water samples are introduced into the autosampler, aligning them properly for subsequent analysis.

Calibration of the instrument is conducted using standard solutions containing known concentrations of chromium (Cr), zinc (Zn), and iron (Fe), facilitating the creation of calibration curves for each metal. Once calibrated, the water samples are analyzed for Cr, Zn, and Fe, with each acidified and prepared sample introduced into

the autosampler. Instrument parameters are adjusted according to polarized Zeeman mode specifications, and the samples are run through the instrument, measuring the absorbance of light at specific wavelengths for each metal. The absorbance values obtained for Cr, Zn, and Fe are meticulously recorded for further analysis.

Quality control measures are implemented throughout the process to ensure the reliability and accuracy of the results. Blank samples and replicate analyses are run alongside the samples to validate the precision of the instrument. Furthermore, the results are verified by analyzing certified reference materials (CRMs) with known concentrations of Cr, Zn, and Fe. The utilization of the polarized Zeeman effect in the Hitachi Model Z-2000 atomic absorption spectrophotometer enhances sensitivity and accuracy in metal analysis, enabling the detection of trace metal levels in the water samples with precision. This comprehensive approach underscores the commitment to scientific rigor and ensures the validity of the analytical results obtained.

Health-related threats were assessed using established protocols. The calculation of daily intake indices (CDI) was conducted following the equation refined by Muhammad et al. (2011)

$$CDI = C \times DI / BW$$

The variable C represents the concentrations of heavy metals ($\mu g/L$), BW denotes body weight, and the water intake on a daily basis is denoted by DI. In the assessment of noncarcinogenic risks, using the below equation, the hazard quotient (HQ) is determined

$$HQ = CDI / RfD$$

The RfD, signifies the acceptable daily intake level for a substance over an extended period without adverse health effects, while CDI represents chronic daily intake. According to the US EPA (1999), the RfD values are approximately $5.0\times10-45.0\times10-4$, $7.0\times10^{-17}.0\times10^{-1}$, $3.0\times10^{-1}3.0\times10^{-1}$, and 1.5 mg kg^{-1} per day for Cd, Fe, Zn, and Cr, respectively. The examination of water samples included assessments of total dissolved solids (TDS), pH levels, electrical conductivity (EC), and temperature at each sampling site. pH measurements were conducted using Mettler

Delta 320 pH meters. Additionally, temperature readings were recorded at the sample sites utilizing Hanna Instruments meters.

CHAPTER 5
RESULTS AND CONCLUSIONS

5.1 Radon

Radon plays an important part in human life, and it has a dual role in it. The radon presence in the soil, rocks, and water has a positive impact and facilitates humans in the identification and prediction of frequent earthquakes, and volcanism and assists in the marking of fault dislocation in the field of hydrological research, while it has also plenty of negative effects on humans due its occurrence in elevated amounts in the drinking water and indoor environment, it can cause a significant health hazard for human life due it carcinogenic effects (Karimdoust et al., 2010). Human beings are commonly exposed to radon through two primary pathways: inhalation and ingestion. Radon can infiltrate indoor environments through cracks and openings in floors and walls, with groundwater serving as an additional source of radon entry (Khan et al., 2014). Within indoor spaces, the short-lived decay products of radon and radon itself, such as 214Po, 214Bi, and 218Po, constitute significant sources of public exposure to natural radioactivity, contributing to nearly 50% of the global average effective dose to communities. Among the daughters of 222Rn that emit alpha particles, 214Po and 218Po collectively contribute to over 90% of the total radiation dose resulting from radon exposure. Upon decay, radon releases energy that can potentially damage DNA in sensitive organs like the lungs and stomach, thereby increasing the risk of cancer (Khan et al., 2014).

At present, the Environmental Protection Agency (EPA) has not set forth precise regulations for radon levels in drinking water. Nonetheless, based on risk evaluations primarily associated with inhalation, the EPA introduced a proposed standard for radon contamination in drinking water. This guideline, referred to as the Maximum Contaminant Level (MCL), suggests a limit of 11.1 Bq l^{-1} (300 pCi l^{-1} or 11.1 kBq m^{-3}) for communal water provisions, based on a transfer ratio of 10^4 to 1 for radon in water to air within domestic settings (Zhou W et al., (2001)).

During laboratory analysis, a comprehensive examination was conducted on 30 water samples sourced from diverse locations. The RAD7 instrument facilitated the measurement of radon concentration in these samples, the findings of which are

meticulously documented in Table 2. Although all samples displayed traces of radon, a considerable portion fell within the permissible limits stipulated by the Environmental Protection Agency (EPA). Nonetheless, it was notable that a subset of samples surpassed the prescribed EPA standards for radon concentration in drinking water.

Table 3: Mean Radon concentration

SAMPLE NO.	LOCATION	CO-ORDINATES	MEAN RN CONCENTRATION BQ/M^3
1	Shnawa Gudikhel Tube well	32°53'08.0"N 71°04'29.0"E	6700
2	Shnawa Gudikhel Tube well	32°53'24.0"N 71°04'38.0"E	6720
3	Shnawa Gudikhel Pressure Pump	32°53'26.0"N 71°04'28.0"E	10040
4	Shnawa Gudikhel Hand Pump	32°53'33.0"N 71°04'28.0"E	6800
5	Shnawa Gudikhel Hand Pump	32°52'40.0"N 71°03'41.0"E	6470
6	Shnawa Gudikhel Pressure Pump	32°52'51.3"N 71°04'06.1"E	5560
7	Shnawa Gudikhel Hand Pump	32°53'58.2"N 71°04'27.4"E	4730
8	Shnawa Gudikhel Tube well	32°52'51.3"N 71°04'06.1"E	5870
9	Shnawa Gudikhel Hand Pump	32°52'13.7"N 71°03'01.9"E	10700
10	Shnawa Gudikhel Hand Pump	32°56'20.0"N 71°04'04.0"E	12760
11	Shnawa Gudikhel Pressure Pump	32°56'38.8"N 71°03'54.5"E	12000
12	Shaheedan Banda Hand Pump	32°55'11.2"N 71°04'44.5"E	9670
13	Shaheedan Banda Tube Well	32°56'53.8"N 71°03'42.3"E	12400
14	Shaheedan Banda Tube Well	32°57'27.2"N 71°03'55.9"E	3850
15	Ganderi Khattak Hand Pump	32°58'10.4"N 71°03'38.6"E	10600
16	Ganderi Khattak Tube Well	32°59'14.7"N 71°03'44.6"E	13100
17	Ganderi Khattak Tube Well	32°59'35.9"N 71°04'00.9"E	8670
18	Ganderi Khattak Pressure Pump	32°57'46.3"N 71°03'40.9"E	8560
19	Takhti-e-Naserati Hand Pump	32°59'57.7"N 71°04'27.0"E	5680
20	Takhti-e-Naserati Pressure Pump	32°59'56.5"N 71°04'49.3"E	2900
21	Takhti-e-Naserati Pressure Pump	33°00'07.2"N 71°05'18.7"E	5600
22	Takhti-e-Naserati Pressure Pump	32°59'54.9"N 71°05'27.0"E	5530
23	Takhti-e-Naserati Hand Pump	33°00'18.7"N 71°05'41.3"E	21300

24	Takhti-e-Naserati Hand Pump	33°00'45.8"N 71°06'00.4"E	8890
25	Takhti-e-Naserati Hand Pump	33°00'42.7"N 71°05'27.0"E	8770
26	Takhti-e-Naserati Hand Pump	33°01'06.1"N 71°06'08.7"E	10600
27	Takhti-e-Naserati Pressure Pump	33°00'29.4"N 71°04'60.0"E	8980
28	Takhti-e-Naserati Tube Well	33°00'50.9"N 71°04'42.7"E	10100
29	Takhti-e-Naserati Tube Well	33°01'10.5"N 71°04'38.5"E	11660
30	Takhti-e-Naserati Pressure Pump	33°01'31.9"N 71°04'10.2"E	13600

5.2 Radon Discussion

In alignment with previous studies conducted in the region, the evaporitic sequence within our study area predominantly comprises Bahadurkhel Salt and Jatta Gypsum formations dating back to the Eocene age. Notably, investigations into radon concentration levels within these formations have yielded insightful data. For instance, the Bahadurkhel Salt formation exhibits varying radon concentrations ranging from 0.15 to 7.6 Bq/L, with an average concentration of 1.8 Bq/L. Similarly, the Jatta Gypsum formation showcases radon levels spanning from 0.2 to 3.4 Bq/L, with an average concentration of 1.6 Bq/L (Khan et al., 2022). These findings provide valuable context for interpreting and contextualizing our results concerning radon concentration within the study area. Building upon previous research findings, our study delves into the radon concentrations within the limestone of the Kohat Formation, attributed to the Eocene age, prevalent in our study area. The Kohat Formation notably exhibits bioclastic limestone in its lower sections, transitioning into massive limestone towards the upper layers. This geological composition is known to influence radon concentration variations within the formation. Radon concentrations within this unit span a considerable range, from 0.43 to 16.5 Bq L^{-1}, with the concentration averaging at 3.3 Bq L^{-1} (Khan et al., 2022). These findings are instrumental in understanding the distribution and behavior of radon within limestone formations, thereby facilitating correlations with groundwater quality and radon contamination levels within the study area.

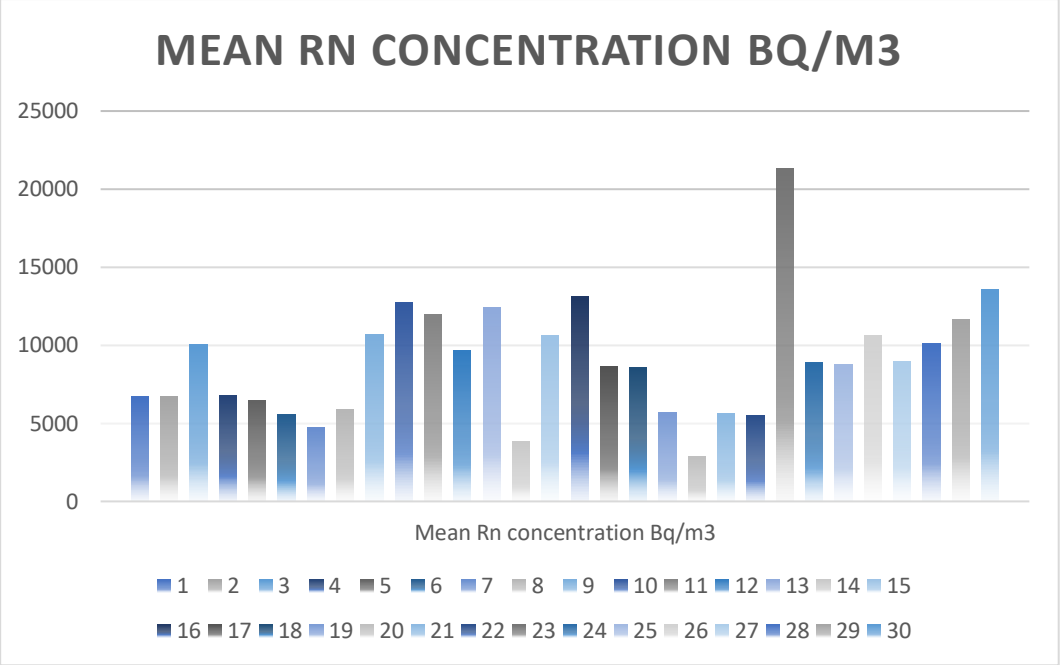

Figure 9: Mean Rn conc shown by histogram

Radon emanates primarily from uranium-rich bedrocks (Esan et al., 2020). Within limestone formations, elevated levels of radon can be attributed to the relatively high concentration of uranium present in carbonates compared to evaporites. The combination of a high surface area of uranium and the bedrock's permeability contributes to increased radon concentrations (Scheib et al., 2013). Typically, uranium exhibits a uniform distribution within limestones, with concentrations usually less than 10 parts per million (ppm), often associated with finely disintegrated organic matter found in bioclastic limestones. This abundance of uranium surface area in limestones, compared to granites, facilitates the effective release of 222Rn into both air and water (Appleton and Ball 1995). However, the migration of radon may encounter restrictions imposed by carbonate cements, which notably diminish both permeability and porosity within the matrix (Scheib et al., 2013).

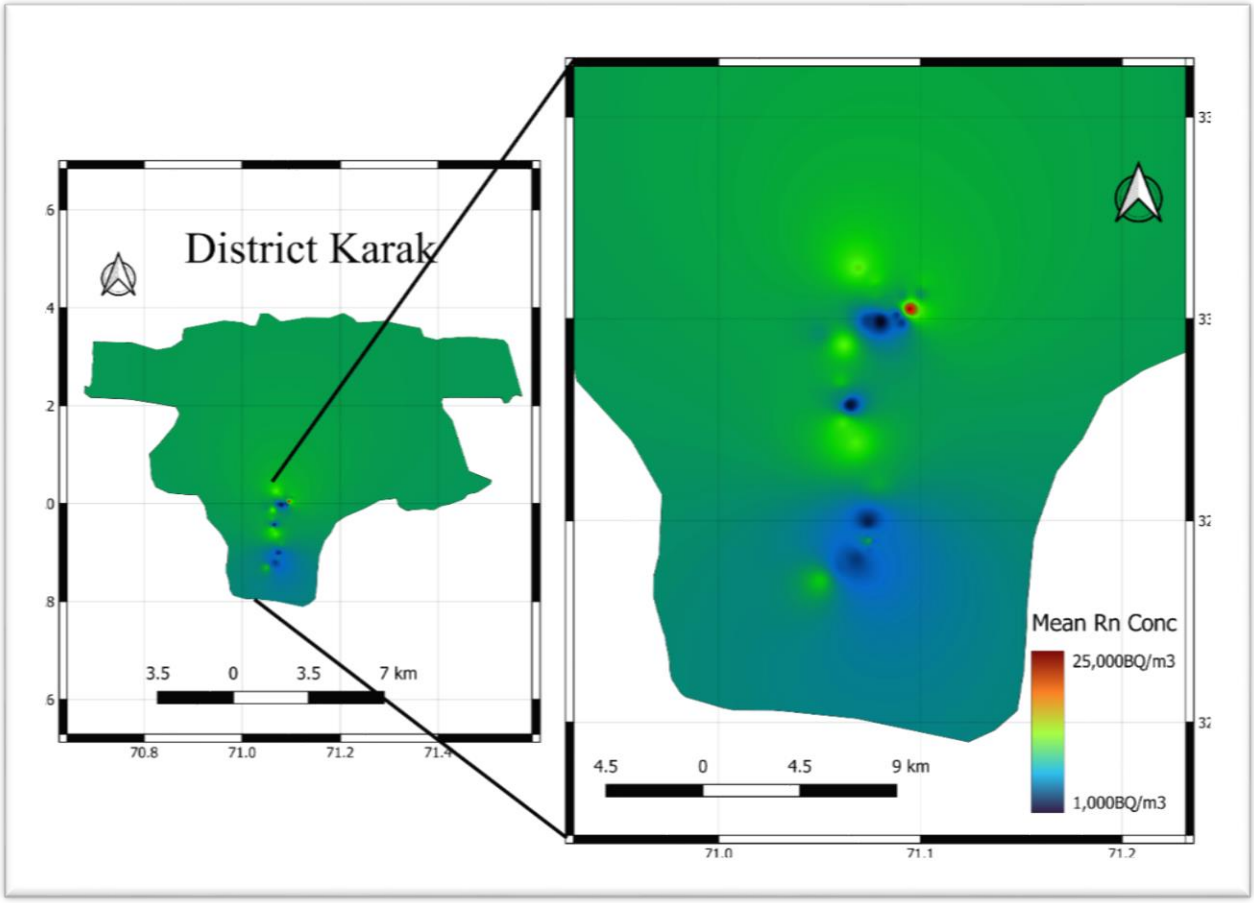

Figure 10: Spatial interpolation map of radon distribution

The radon concentrations in 30 drinking water samples collected from the study area have been assessed. Additionally, the mean annual effective doses to the stomach, lung, and whole body per individual for adults have been analyzed and are shown in Table 3. Among the samples, 3 out of 9 from tube wells, 2 out of 9 from pressure pumps, and 2 out of 11 from hand pumps exhibit radon concentrations surpassing the Maximum Contaminant Level (MCL) of 11.1 Bq/L. This indicates that 33% of tube well samples, 23% of pressure pumps, and 18% of hand pump samples have radon levels exceeding the EPA's recommended threshold. On average, 24% of drinking water samples from the area under study exceed the EPA's MCL.

Table 4: Mean annual effective doses

SAMPLE LOCATION	MEAN	INGESTION	INHALATION	TOTAL EFFECTIVE DOSE
SHNAWA GUDIKHEL TUBE WELL	6700	0.0014	0.017	**0.018**
SHNAWA GUDIKHEL TUBE WELL	6720	0.0014	0.017	**0.018**
SHNAWA GUDIKHEL PRESSURE PUMP	10040	0.0021	0.025	**0.027**
SHNAWA GUDIKHEL HAND PUMP	6800	0.0014	0.017	**0.018**
SHNAWA GUDIKHEL HAND PUMP	6470	0.0014	0.016	**0.017**
SHNAWA GUDIKHEL PRESSURE PUMP	5560	0.0012	0.014	**0.015**
SHNAWA GUDIKHEL HAND PUMP	4730	0.0010	0.012	**0.013**
SHNAWA GUDIKHEL TUBE WELL	5870	0.0012	0.015	**0.016**
SHNAWA GUDIKHEL HAND PUMP	10700	0.0022	0.027	**0.029**
SHNAWA GUDIKHEL HAND PUMP	12760	0.0027	0.032	**0.034**
SHNAWA GUDIKHEL PRESSURE PUMP	12000	0.0025	0.030	**0.032**
SHAHEEDAN BANDA HAND PUMP	9670	0.0020	0.024	**0.026**
SHAHEEDAN BANDA TUBE WELL	12400	0.0026	0.031	**0.034**
SHAHEEDAN BANDA TUBE WELL	3850	0.0008	0.010	**0.010**
GANDERI KHATTAK HAND PUMP	10600	0.0023	0.027	**0.029**
GANDERI KHATTAK TUBE WELL	13100	0.0028	0.032	**0.035**
GANDERI KHATTAK TUBE WELL	8670	0.0018	0.022	**0.024**
GANDERI KHATTAK PRESSURE PUMP	8560	0.0018	0.022	**0.024**
TAKHTI-E-NASERATI HAND PUMP	5680	0.0012	0.014	**0.015**
TAKHTI-E-NASERATI PRESSURE PUMP	2900	0.0006	0.008	**0.0086**
TAKHTI-E-NASERATI PRESSURE PUMP	5600	0.0012	0.014	**0.015**
TAKHTI-E-NASERATI PRESSURE PUMP	5530	0.0012	0.014	**0.015**
TAKHTI-E-NASERATI HAND PUMP	21300	0.0044	0.054	**0.058**
TAKHTI-E-NASERATI HAND PUMP	8890	0.0019	0.022	**0.024**
TAKHTI-E-NASERATI HAND PUMP	8770	0.0018	0.022	**0.024**
TAKHTI-E-NASERATI HAND PUMP	10600	0.0022	0.027	**0.029**

TAKHTI-E-NASERATI PRESSURE PUMP	8980	0.0019	0.023	**0.025**
TAKHTI-E-NASERATI TUBE WELL	10100	0.0021	0.025	**0.027**
TAKHTI-E-NASERATI TUBE WELL	11660	0.0022	0.029	**0.031**
TAKHTI-E-NASERATI PRESSURE PUMP	13600	0.0029	0.034	**0.037**

Considering insights from previous studies by Khan et al. (2022) on fault and thrust systems, particularly the Garori thrust, our analysis revealed an extensive range in the radon values of the studied profiles, ranging from 1.1 Bq/l to 51 Bq/l. Across the Garori fault, radon concentrations peaked as the fault zone approached and gradually declined away from the fault zone. Additionally, concentrations showed a broad spectrum in wider fault zones, while narrow fault zones exhibited narrow concentration peaks. Similar results are shown for Karak Thrust with radon concentration from (0.15 Bq/l) to (21 Bq/l) the fault revealing the highest concentration in almost all the traverses for K. This observation suggests a potential correlation between fault activity and groundwater radon levels and Metakhel thrust had radon concentrations across all profiles with a range from 0.44 Bq/l to 19 Bq/l, with two extremes observed and the highest readings concentrated at the center, indicated by a distance of 0 meters from the fault.

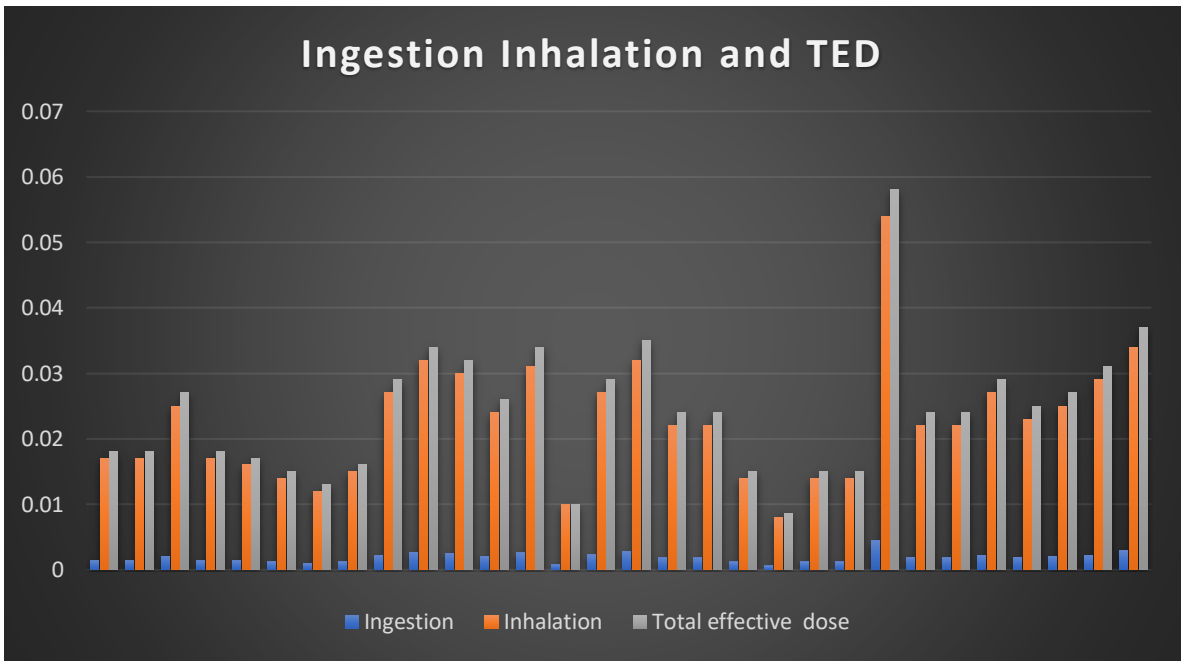

Figure 11: Ingestion, Inhalation, and Total Effective Dose Histogram

5.3 Chromium, Zinc, and Iron Results

Both natural and human activities contribute to the pollution of drinking water sources. Bedrocks, as a natural factor, have a substantial impact on water composition, whereas human activities such as industrial discharge, sewage release, and agricultural runoff also contribute (Nawab et al., 2016). These sources introduce into water bodies a notable quantity of both necessary and unnecessary harmful elements (Santos et al., 2005; Kumar et al., 2015).

Utilization of wastewater from households and industries for agricultural purposes has led to a deterioration in groundwater quality, rendering it unsuitable for consumption (Nasir et al., 2012). Trace elements are consistently introduced into water bodies through anthropogenic and natural activities, with some being essential while others are non-essential. Among the common elements found in water are As, Ca, Mn, Mo, Na, Ni, Pb, Se Cd, Co, Zn, Cu, Fe, Hg, K, Mg, and Cr. Elements like K, Na, Mg, Ca, Mn, Fe, Zn, and Co are crucial for living organisms in various quantities (Hussein et al., 2005).

Table 5: Concentration of Fe, Zn, and Cr in ppm and ppb

SAMPLE NO.	LOCATION	TEMP ^{O}C	pH	TDS mg/l	Cr ppm	Fe ppm	Zn ppb
1	Shnawa Gudikhel Tube well	21°	7.40	875	0.05	0.05	51
2	Shnawa Gudikhel Tube well	22°	7.27	1690	0.6	0.071	37
3	Shnawa Gudikhel Pressure Pump	21°	7.09	2144	0.07	0.041	46
4	Shnawa Gudikhel Hand Pump	24°	7.30	984	0.02	0.070	52
5	Shnawa Gudikhel Hand Pump	23°	8.60	331	0.03	0.015	46
6	Shnawa Gudikhel Pressure Pump	22°	7.20	574	0.05	0.131	50
7	Shnawa Gudikhel Hand Pump	20°	7.31	210	0.05	0.113	40
8	Shnawa Gudikhel Tube well	19°	7.65	495	0.04	0.050	35
9	Shnawa Gudikhel Hand Pump	20°	7.60	150	0.04	0.052	42
10	Shnawa Gudikhel Hand Pump	21°	7.70	624	0.02	0.059	41
11	Shnawa Gudikhel Pressure Pump	19°	7.43	324	0.03	0.075	43
12	Shaheedan Banda Hand Pump	21°	7.49	334	0.08	0.134	25

13	Shaheedan Banda Tube Well	23 º	8.10	234	0.06	0.082	41
14	Shaheedan Banda Tube Well	21 º	8.52	320	0.7	0.065	39
15	Ganderi Khattak Hand Pump	20 º	7.45	378	0.04	0.049	26
16	Ganderi Khattak Tube Well	23 º	7.72	456	0.03	0.051	36
17	Ganderi Khattak Tube Well	19 º	7.70	201	0.04	0.046	49
18	Ganderi Khattak Pressure Pump	15 º	7.65	297	0.05	0.110	43
19	Takhti-e-Naserati Hand Pump	19 º	7.74	400	0.02	0.071	31
20	Takhti-e-Naserati Pressure Pump	20 º	7.65	389	0.04	0.041	36
21	Takhti-e-Naserati Pressure Pump	17 º	7.55	487	0.07	0.047	51
22	Takhti-e-Naserati Pressure Pump	21 º	8.12	689	0.06	0.039	42
23	Takhti-e-Naserati Hand Pump	22 º	7.35	1087	0.04	0.105	41
24	Takhti-e-Naserati Hand Pump	19 º	7.21	784	0.05	0.081	24
25	Takhti-e-Naserati Hand Pump	18 º	7.32	68	0.07	0.042	30
26	Takhti-e-Naserati Hand Pump	21 º	7.10	280	0.04	0.092	33
27	Takhti-e-Naserati Pressure Pump	20 º	7.03	276	0.03	0.056	47
28	Takhti-e-Naserati Tube Well	18 º	8.34	471	0.07	0.094	43
29	Takhti-e-Naserati Tube Well	20 º	7.21	663	0.05	0.061	37
30	Takhti-e-Naserati Pressure Pump	19 º	7.24	628	0.04	0.040	26

Fluctuations in the levels of various elements within water samples across diverse locations and sources can be attributed to several factors. These may include variances in geographical and geological features, pollution levels, specific sources of sample collection, prevailing climatic conditions, and human activities. Common sources of water samples encompass wells, tube wells, hand pumps, and pressure pumps.

The pH level of an environment significantly influences certain mineral's precipitation. For instance, Calcium carbonate ($CaCO3$) does not precipitate in acidic environments but requires an alkaline medium for precipitation, with temperature also playing a crucial role (Reincek et al., 1975). In our area of study, the pH ranges from acidic to slightly alkaline, spanning between 7.10 and 8.60. Specifically, in tube wells,

pH levels range from 6.69 to 8.4, with a mean value of 7.60. Hand pumps exhibits pH levels ranging from 7.10 to 8.60, with a mean value of 8.00. Samples collected from pressure pumps demonstrate pH levels ranging from 7.7 to 8.12, with a mean of 7.97. The highest pH value recorded is 8.6 found in the Shnawa GudiKhel hand pump. While the lowest is 7.10 recorded in Takht-I-Naserati hand pump.

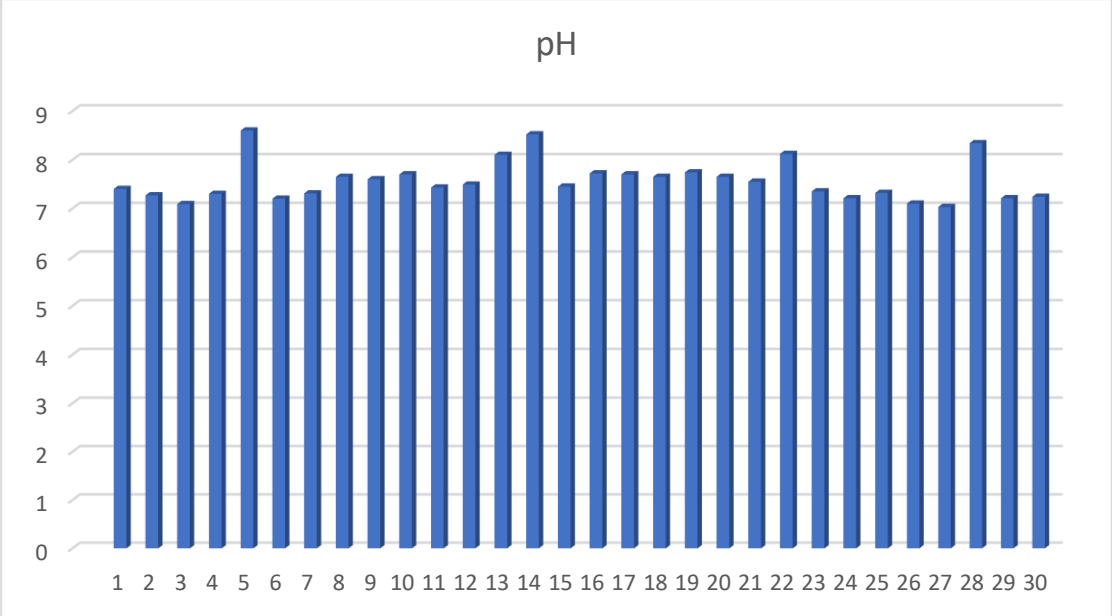

Figure 12: Samples pH recorded in the study area

The Total Dissolved Solids (TDS) measurements of drinkable water samples collected from diverse sources (e.g., hand pumps, Pressure pumps, tube wells) to the WHO's 2008 standards, most samples fell within permissible limits, except for three samples with significantly higher TDS values. Notably, the average Total Dissolved Solids (TDS) concentration in water obtained from hand pumps was marginally higher compared to that from tube wells, springs, and streams. Analysis of TDS levels in water samples extracted from tube wells indicated concentrations spanning from 201 mg/l to 1690 mg/l. Conversely, TDS values in samples of water sourced from hand pumps exhibited variability ranging between 68 mg/l and 1087 mg/l. Pressure pump samples exhibited TDS values ranging from 276 mg/l to 2144 mg/l. The highest TDS concentration of 2144 mg/l was recorded in sample 03 from Shnawa GudiKhel pressure pump, while the lowest value of 68 mg/l was observed in sample 25 from the Takht-I-Naserati hand pump.

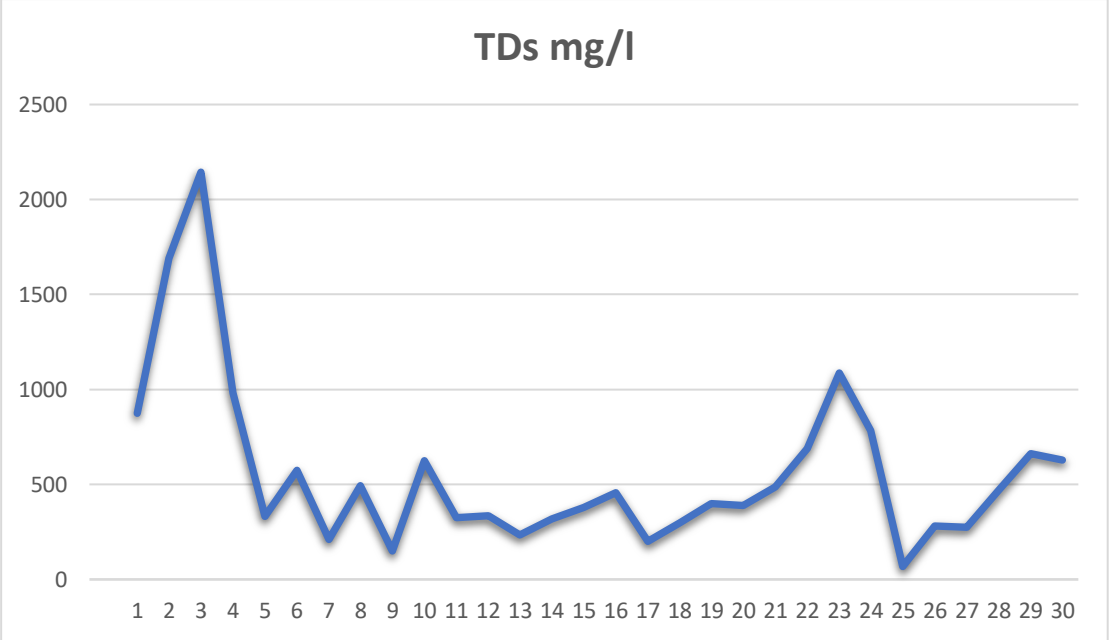

Figure 13: TDS on a histogram chart

In water samples of tube wells, the Cr concentration ranges from 0.020 ppm to 0.7 ppm, with a mean recorded value of 0.06 ppm. For hand pump samples, the Cr concentration ranges from 0.02 ppm to 0.08 ppm, resulting in an average of 0.06 ppm. In the samples that were taken from pressure pumps, chromium concentrations ranged from 0.03 ppm to 0.07 ppm, with an average of 0.065 ppm. Samples collected from tube wells exhibit Cr concentrations ranging from 0.03 ppm to 0.7 ppm, with the highest observed concentration at 0.7 ppm and the lowest at 0.02 ppm, resulting in a mean of 0.045 ppm.

Samples taken from tube wells in Tehsil Karak show chromium (Cr) Chronic Daily Intake values ranging from 0.021 to 0.51 µg kg^{-1}day, with an average of 0.019 µg kg^{-1}-day. In contrast, samples from hand pumps in the study area indicate CDI values for Cr ranging from 0.01 to 0.57 µg kg^{-1}-day, with a mean value of 0.0195 µg kg^{-1}day. Pressure pump water samples reveal CDI values for Cr between 0.01 and 0.45 µg kg^{-1}day, with an average of 0.0132 µg kg^{-1}day. Additionally, water samples from tube wells exhibit Cr concentrations ranging from 0.01 to 0.36 µgkg^{-1}day, with a mean value of 0.0105µgkg^{-1}day.

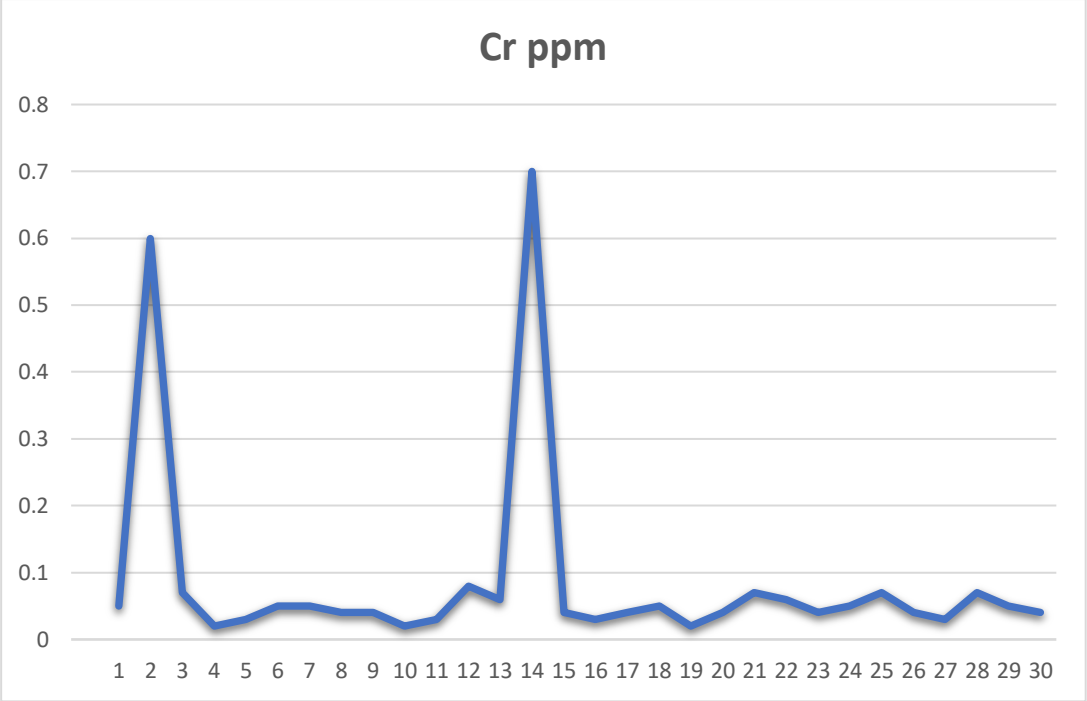

Figure 14: Cr concentration shown on a histogram

In water samples obtained from tube wells in Tehsil Karak, the concentration of Fe ranges from 0.01 ppm to 0.134 ppm, with a mean of 0.075 ppm. For samples sourced from pressure pumps, Fe concentrations range from 0.03 ppm to 0.131 ppm, resulting in a mean of 0.092 ppm. Hand pump samples exhibit Fe concentrations ranging from 0.015 ppm to 0.134 ppm, yielding a mean of 0.065 ppm. Among the water samples, the highest Iron concentration is recorded at 0.134 ppm in sample no. 12 sourced from a tube well in Shaheedan Banda. The lowest Fe concentration observed is 0.010 ppm in sample no. 5, sourced from tube wells in the village Shanwa GudiKhel. The levels of iron (Fe) in drinking water sources comply with the acceptable standards set by the WHO (2008).

The chronic daily intake values for iron in various water sources show considerable variation. In tube well water, CDI values range from 0.02 to 2.22 µg/kg-day, with a mean of 0.699 µg/kg-day. Similarly, pressure pump water samples exhibit CDI values for Fe ranging from 0.01 to 1.64 µg/kg-day, averaging at 0.648 µg/kg-day. Hand pump water samples show Fe levels ranging from 0.01 to 0.25 µg/kg-day, with a mean value of 0.0459 µg/kg-day

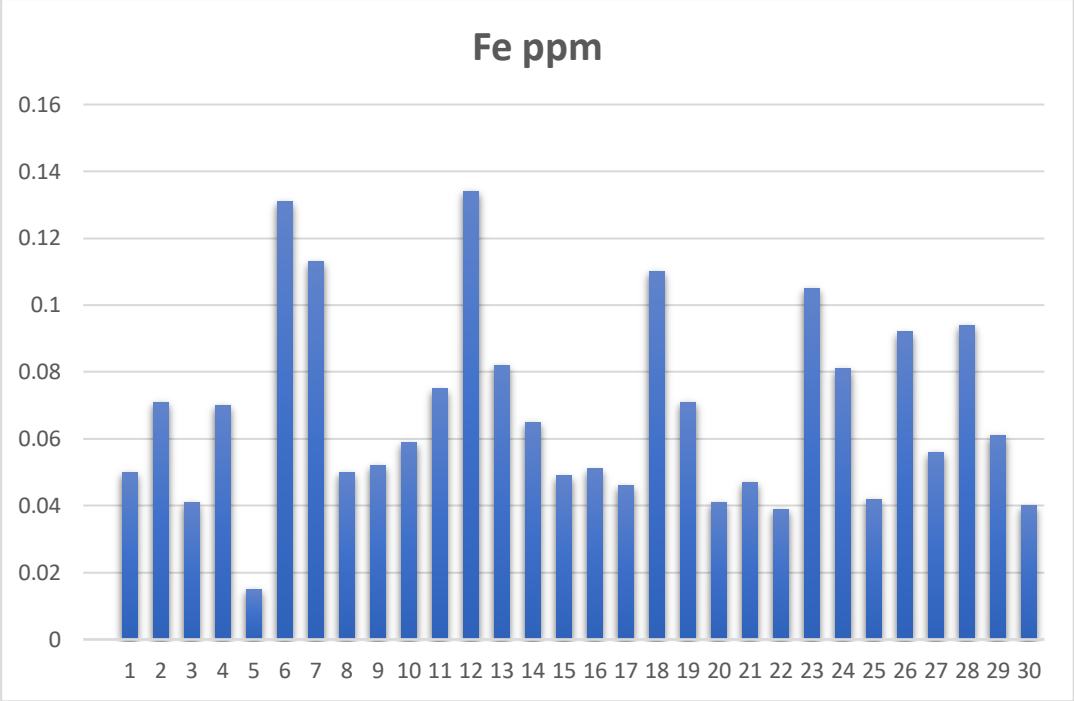

Figure 15: Fe Concentration labelled on a histogram

The concentration of Zn in the water samples acquired from tube wells in the study area varies from 35 ppb to 51 ppb, with a mean of 43 ppb. For pressure pump samples, the Zn concentration falls within the range of 26 ppb to 51 ppb, with a mean of 38.5 ppb. Hand pump samples show Zn concentrations ranging from 24 ppb to 52 ppb, with an average of 38 ppb. The concentrations of Zinc in all of the samples used for drinking purposes fall inside their respective accepted ranges, as per the values which are outlined by WHO (2008).

The computed CDI values for water samples extracted from tube wells show zinc concentrations spanning from 0.27 to 22.55 µg/kg-day, with an average of 2.155 µg kg^{-1}day. Conversely, in pressure pumps, zinc chronic daily intake values range from 0.25 to 61.8 µg kg^{-1}day, with a mean of 13.025 µg kg^{-1}day. Tube wells indicates zinc CDI values ranging between 0.02 and 0.25 µg kg^{-1}day, with a mean of 0.0475 µg/kg-day. Hand pump samples display zinc CDI values from 0.23 to 35.6 µg kg^{-1}day, with an average of 14.563 µg kg^{-1}day.

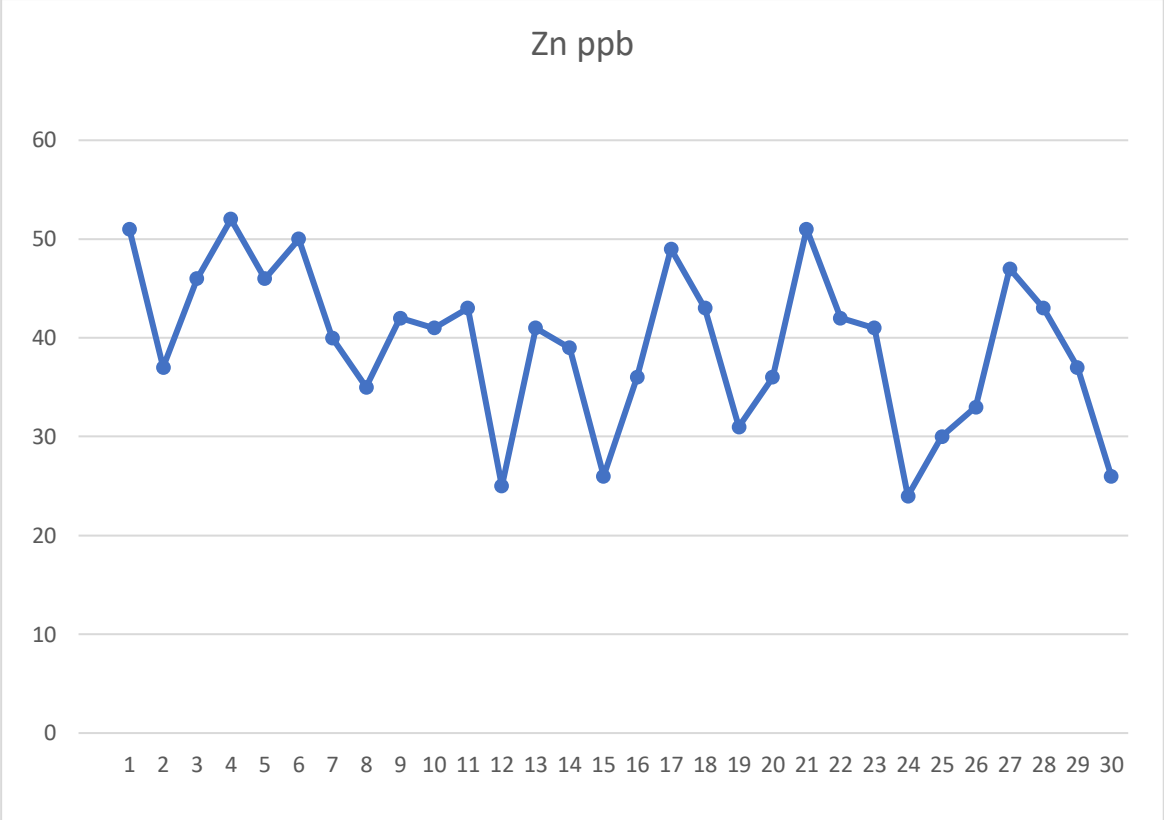

Figure 16: Zinc concentration shown on histogram

Conclusions

The study area had the concentration of radon in the tested water samples remained comfortably below the Environmental Protection Agency's (EPA) Maximum Contaminant Level (MCL) threshold. However, it's noteworthy that approximately a quarter, specifically 24%, of the water samples did surpass this regulatory limit. This finding aligns with prior scholarly works which have posited that regions characterized by fault lines and distinct geological formations tend to exhibit elevated concentrations of radon gas. The intricate interplay between these geological features and the percolation of water from the surface downwards can potentially lead to groundwater contamination by radon.

The implications of such contamination are substantial, particularly for the local populace whose primary source of drinkable water is groundwater. The pervasive presence of radon gas in proximity to these water sources poses a significant risk, gradually escalating the potential for waterborne contamination. Consequently, there arises an imperative to implement robust purification methods to ensure the provision of safe and uncontaminated water to the community.

The ramifications of radon's presence on residents cannot be overstated. With their dependence on groundwater for everyday consumption needs, the exacerbation of radon contamination poses a direct threat to public health and well-being. The cumulative effect of prolonged exposure to radon-laden water can lead to a host of adverse health outcomes, ranging from respiratory issues to more severe long-term health complications.

Considering these findings, it becomes evident that proactive measures must be taken to mitigate the risks associated with radon contamination in groundwater sources. This necessitates a multifaceted approach, encompassing not only rigorous monitoring and assessment protocols but also the implementation of advanced water purification technologies tailored to effectively neutralize radon concentrations. Furthermore, community awareness and education initiatives play a pivotal role in fostering a collective understanding of the risks posed by radon contamination and promoting proactive engagement in safeguarding public health.

In summary, the documented presence of radon in groundwater sources within the study area underscores the pressing need for concerted action to safeguard the health and well-being of local communities. By prioritizing robust monitoring, mitigation, and community engagement efforts, it is possible to mitigate the adverse effects of radon contamination and ensure the provision of safe and potable water resources for generations to come.

The mean concentration levels of both pH and Total Dissolved Solids (TDS) in the water samples are observed to be within admissible limits, indicating satisfactory water quality overall. However, it is noteworthy that in three samples, the concentrations of pH and TDS exceed the permissible limits set by the World Health Organization (WHO) in 2008, suggesting potential concerns regarding water quality in those specific cases.

Furthermore, the concentrations of heavy minerals examined in the study fall within the non-toxic range, providing assurance of minimal risk associated with exposure to these substances. Additionally, concentrations of heavy metals such as zinc (Zn), iron (Fe), and chromium (Cr) are observed to be within acceptable limits compared to the WHO's fixed values from 2008, indicating a lower likelihood of health risks linked with heavy metal contamination in the water sources.

Moreover, the Hazard Quotient (HQ) and Chronic Daily Intake (CDI) indices calculated for the heavy metals in samples collected from a segment of Tehsil Karak reveal an order of concern, with Zn posing the highest risk followed by Fe and then Cr. However, it's important to note that these indices collectively indicate that there are no significant health risks posed to the local inhabitants from exposure to these heavy metals.

In summary, while there are instances where certain parameters exceed recommended limits, overall water quality appears to be within acceptable ranges. Continuous monitoring, coupled with targeted interventions where necessary, is essential to ensure the continued provision of safe drinking water to the local population.

Chapter 6

DISCUSSIONS

Radon is predominantly sourced from uranium-rich bedrock, as highlighted by Esan et al. (2020). In limestone formations, heightened levels of radon are often linked to the relatively elevated concentration of uranium within carbonates, surpassing that of evaporites. The interaction between a substantial uranium surface area and the permeability of the bedrock contributes to the augmentation of radon concentrations, as indicated by Scheib et al. (2013). Typically, uranium is uniformly distributed within limestones, with concentrations usually below 10 parts per million (ppm), commonly associated with finely disintegrated organic matter present in bioclastic limestones. This abundance of uranium surface area in limestones, compared to granites, facilitates the efficient release of 222Rn into both air and water, as discussed by Appleton and Ball (1995). However, the migration of radon may encounter hindrances imposed by carbonate cements, significantly reducing both permeability and porosity within the matrix, as emphasized by Scheib et al. (2013). Various factors can influence soil radon activity, including (i) the concentration of parent radionuclides in different rock formations; and (ii) the ratio of volume to surface area of soil and sub-soil particles, where a lower ratio may impede radon escape from the rock matrix; (iii) the average bulk permeability and type of permeability (secondary or primary) of subsurface rocks; and (iv) variations in deep gas flux leading to changes in transport mechanisms driven by advection, as discussed by Singh et al. (2002).

The high concentration of radon in the water samples collected from the Shanawa Gudi Khel area might be due to the presence of uranium-rich dhok Pathan formation. These elevated levels are restricted to some particular areas in the Shanawah Guddikhel village and Takht e Naserati area. Based on the findings of this study, it is evident that radon concentration was high in the wells drilled near or in the uranium-rich bedrocks which were exceeding the safe limits set by the World Health Organization (WHO) for human consumption. The presence of abundant radon in drinking water samples collected from Tehsil Takht-e-Nasrati, specifically in Shanawa Gudi Khel and its surrounding areas, raises concerns regarding the safety of these water sources for drinking purposes. The heightened levels of uranium are likely attributed to the significant uranium-rich formation in the area which is Dhok Pathan Formation.

The study findings indicate that the concentrations of heavy minerals generally remain within non-toxic ranges, suggesting minimal health risks associated with exposure to these substances. Moreover, levels of heavy metals such as zinc (Zn), iron (Fe), and chromium (Cr) typically conform to acceptable limits set by the WHO in 2008. However, it's noteworthy that certain samples exhibit higher concentrations, underscoring the need for further investigation into potential localized contamination sources.

In the study area, the presence of Siwaliks and river deposits significantly contributes to elevated concentrations of iron, zinc, and chromium in drinking water. The Siwalik formations, characterized by sedimentary rocks of varying compositions, contain minerals rich in these metals. Over time, weathering and erosion processes release these minerals into the surrounding environment, including rivers and groundwater. Additionally, river deposits play a crucial role in transporting sedimentary material containing iron, zinc, and chromium from upstream areas to downstream regions. As these rivers traverse through diverse geological formations, they accumulate and carry a variety of metallic ions, augmenting the concentrations of iron, zinc, and chromium in the water bodies of the region. Consequently, the combined influence of Siwaliks and river deposits significantly contributes to the high levels of these metals observed in the study area.

References

Adler, G., Nędzarek, A., & Tórz, A. (2019). Concentrations of selected metals (Na, K, Ca, mg, FE, CU, Zn, al, Ni, PB, cd) in coffee. Slovenian Journal of Public Health, 58(4), 187-193.

Ahmad, S., Ali., A., Khan, M.I., 2005. Imprints of transtensional deformation along Kalabagh Fault in the vicinity of Kalabagh Hills, Pakistan. Pakistan Journal of Hydrocarbon Research, 15, 35- 42.

Ahmad, Sajjad, et al. "Assessment of drinking water quality and human health risks in Karak and adjoining areas, Southeastern Kohat Basin, Pakistan." *Journal of Himalayan Earth Science* 53.1 (2020).

Ahmad, Sajjad, et al. "Joints/Fractures analyses of Shinawah area, District Karak, Khyber Pakhtunkhwa, Pakistan." Journal of Himalayan Earth Sciences 50.2 (2017): 93-113.

Ahmed, Noor, et al. "Prediction of Paleoclimate of Eocene Salt, Kohat Basin, Khyber Pakhtunkhwa, Pakistan." Episodes Journal of International Geoscience 46.1 (2023): 69-84.

Akhtar, Shamim et al. "URANIUM DEPOSITS AND RESOURCES POTENTIAL IN PAKISTAN: A REVIEW." (2015).

Ali, A., 2010. Structure analysis of the trans- indus ranges: implications for the hydrocarbon potential of the NW Himalayas, Pakistan. Unpublished Ph.D. Thesis, University of Peshawar.

Isinkaye, M. O., Matthew-Ojelabi, F., Adegun, C. O., Fasanmi, P. O., Adeleye, F. A., & Olowomofe, O. G. (2021). Annual effective dose from 222 Rn in groundwater of a Nigeria University campus area. Applied Water Science, 11, 1-10.

Ityel, D. (2011). Ground water: Dealing with iron contamination. Filtration & Separation, 48(1), 26-28.

Jaume, S., Lillie, R., 1988. Mechanics of the Salt Range, Potwar Plateau, Pakistan: a fold and thrust belt underlain by evaporites. Tectonics, 5, 57-71.

Jaumé, S.C., and Lillie, R.J., 1988, Mechanics of the Salt Range-Potwar Plateau, Pakistan: A fold-and-thrust belt underlain by evaporites. Tectonics, v. 7, pp. 57−71.

Javed, Tehseen, et al. "Evaluation of groundwater quality in district Karak Khyber Pakhtunkhwa, Pakistan." *Water Science* 33.1 (2019): 1-9.

Kabata-Pendias, Alina. *Trace elements in soils and plants*. CRC press, 2000.

Khan, M.A., Ahmed, R., Raza, H.A., and Kemal, A., 1986, Geology of petroleum in Kohat-Potwar depression, Pakistan. AAPG bulletin, v. 70, pp. 396−414.

Khan, M.A., Ahmed, R., Raza, H.A., Kemal, A 1986. Geology of petroleum in Kohat-Potwar depression, Pakistan. American Association of Petroleum Geologists (AAPG). Bulletin, 70, 396-414.

Khan, Mumtaz Ali, Nimat Ullah Khattak, and Muhammad Hanif. "Radon emission along faults: a case study from district Karak, Sub-Himalayas, Pakistan." Journal of Radioanalytical and Nuclear Chemistry 331.5 (2022): 1995-2003.

Khattak, N. U., et al. "Radon concentration in drinking water sources of the region adjacent to a tectonically active Karak Thrust, southern Kohat Plateau, Khyber Pakhtunkhwa, Pakistan." *Journal of Radioanalytical and Nuclear Chemistry* 302 (2014): 315-329.

Khattak, Nimat Ullah, et al. "Recognition and characterization of a tectonically active Karak Thrust using radon measurement technique in the Southern Kohat Plateau, Pakistan." Journal of Himalayan Earth Sciences 49.2 (2016): 40-49.

Lillie, R.J., Johnson, G.D., Yousuf, M., Zamin, A.S.H., and Yeats, R.S., 1987, Structural development within the Himalayan foreland fold-andthrust belt of Pakistan.

Meissner Jr, Charles R., et al. Stratigraphy of the Kohat quadrangle, Pakistan. No. 716-D. US Govt. Print. Off.,, 1974.

National Water Quality Monitoring Programme. Pakistan Council of Research in Water Resources (PCRWR), Islamabad, Pakistan, 2007.

Noulas, C., Tziouvalekas, M., & Karyotis, T. (2018). Zinc in soils, water and food crops. *Journal of Trace Elements in Medicine and Biology*, *49*, 252-260.

Shimasaki, Akihiro. "Pakistan: Khyber Pakhtunkhwa Water Resources Development Project." (2017).

Ullah, Hussain, et al. "Estimation of uranium concentration in drinking water sources of Tehsil Takht-e-Nasrati, District Karak, Khyber Pakhtunkhwa, Pakistan using fission track technique." *Journal of the Chemical Society of Pakistan* 35 (2013).

Ullah, Z., Li, J.W., Robinson, P.T., Wu, W.W., Khan, A., Dac, N.X., and Adam, M.M.A., 2020, Mineralogy and geochemistry of peridotites and chromitites in the Jijal Complex ophiolite along the Main Mantle Thrust (MMT or Indus Suture Zone) North Pakistan. Lithos, v. 366, 105566.

Ullah, Z., Shah, M.T., Siddiqui, R.H., Lian, D.Y., and Khan, A., 2020, Petrochemistry of high-Cr and high-Al chromitites occurrences of dargai complex along indus suture zone, northern Pakistan. Episodes, v. 43, pp. 689−709.

W. Chesworth, Geochemistry of micronutrients, in: J.J. Mortvedt, F.R. Cox, L.M. Shuman, R.M. Welch (Eds.), Micronutrients in Agriculture, second ed., Soil Sci. Soc. Am. Inc., Madison, WI, 1991, pp. 1–30.

World Health Organization. (2020). *Chromium in Drinking water* (No. WHO/HEP/ECH/WSH/2020.3). World Health Organization.

Sarmad MS Geo

by Mumtaz Ali Khan

Submission date: 01-Mar-2024 07:09PM (UTC+0500)
Submission ID: 2278825781
File name: Thesis_File_final.docx (6.96M)
Word count: 14469
Character count: 82316

INVESTIGATION OF RADON, CHROMIUM, ZINC, AND IRON IN DRINKING WATER SOURCES AND ITS HEALTH IMPACTS IN THE SOUTH OF KARAK CITY KARAK, KPK, PAKISTAN

By

Sarmad Aali Shan Haider

Department of Earth and Environmental Sciences Bahria University, Islamabad Pakistan

2024

Sarmad MS Geo

ORIGINALITY REPORT

15%	11%	11%	4%
SIMILARITY INDEX	INTERNET SOURCES	PUBLICATIONS	STUDENT PAPERS

PRIMARY SOURCES

1	nceg.uop.edu.pk Internet Source	2%
2	Submitted to Higher Education Commission Pakistan Student Paper	2%
3	www.frontiersin.org Internet Source	2%
4	link.springer.com Internet Source	2%
5	pt.scribd.com Internet Source	1%
6	Mumtaz Ali Khan, Nimat Ullah Khattak, Muhammad Hanif. "Radon emission along faults: a case study from district Karak, Sub-Himalayas, Pakistan", Journal of Radioanalytical and Nuclear Chemistry, 2022 Publication	1%
7	N. U. Khattak, M. A. Khan, M. T. Shah, N. Ali. "Radon concentration in drinking water sources of the region adjacent to a	1%

tectonically active Karak Thrust, southern Kohat Plateau, Khyber Pakhtunkhwa, Pakistan", Journal of Radioanalytical and Nuclear Chemistry, 2014
Publication

8	f1000research.com Internet Source	<1 %
9	Tehseen Javed, Tahir Sarwar, Ihsan Ullah, Shakeel Ahmad, Sadaf Rashid. "Evaluation of groundwater quality in district Karak Khyber Pakhtunkhwa, Pakistan", Water Science, 2019 Publication	<1 %
10	www.researchgate.net Internet Source	<1 %
11	S. Ahmad, D. Kroon, J. J. G. Reijmer, S. Khan, O. S. Hersi, B. Wadood. "Paleogene carbonate ramp development in the Kohat Basin of northwestern Pakistan", Australian Journal of Earth Sciences, 2023 Publication	<1 %
12	E. Srinivasa, D. R. Rangaswamy, J. Sannappa. "Measurement of Radon Concentration and Evaluation of Total Dose in Drinking Water of Chikmagalur City, Karnataka", Journal of the Geological Society of India, 2019 Publication	<1 %

13	Mumtaz Ali Khan, Nimat Ullah Khattak, Muhammad Hanif, Nadhir Al-Ansari, Muhammad Bashir Khan, Muhsan Ehsan, Ahmed Elbeltagi. "Health risks associated with radon concentrations in carbonate and evaporite sequences of the uranium-rich district Karak, Pakistan", Frontiers in Environmental Science, 2022 Publication	<1 %
14	assets.researchsquare.com Internet Source	<1 %
15	www.dws.gov.za Internet Source	<1 %
16	Submitted to University of Ulster Student Paper	<1 %
17	academics.su.edu.krd Internet Source	<1 %
18	www.yumpu.com Internet Source	<1 %
19	Abbasi, I.A.. "Thrust kinematics in the Kohat Plateau, Trans Indus Range, Pakistan", Journal of Structural Geology, 1991 Publication	<1 %
20	Habila Nuhu, Suhairul Hashim, Mohamad Syazwan Mohd Sanusi, Muneer Aziz Saleh. "Radon activity concentration measurements	<1 %

	in water sources from Perak state Malaysia", Journal of Radiation Research and Applied Sciences, 2020 Publication	
21	joinus.pk Internet Source	<1 %
22	www.enfo.hu Internet Source	<1 %
23	Saleemi, A.A.. "Mineral and chemical composition of Karak mudstone, Kohat Plateau, Pakistan: implications for smectite-illitization and provenance", Sedimentary Geology, 200002 Publication	<1 %
24	www.toronto.ca Internet Source	<1 %
25	makhillpublications.co Internet Source	<1 %
26	Submitted to Mount Kenya University Student Paper	<1 %
27	dspace.nm-aist.ac.tz Internet Source	<1 %
28	www.legislation.qld.gov.au Internet Source	<1 %
29	www.zora.uzh.ch Internet Source	<1 %

30	zankojournal.su.edu.krd Internet Source	<1 %
31	Christos Noulas, Miltiadis Tziouvalekas, Theodore Karyotis. "Zinc in soils, water and food crops", Journal of Trace Elements in Medicine and Biology, 2018 Publication	<1 %
32	Ugwu Chidiebere Emmanuel, Maduka Ignatius Chukwudi, Suru Stephen Monday, Anakwuo Ikechukwu Anthony. "Human health risk assessment of heavy metals in drinking water sources in three senatorial districts of Anambra State, Nigeria", Toxicology Reports, 2022 Publication	<1 %
33	www.sciencepublishinggroup.com Internet Source	<1 %
34	R.C. Ramola. "Occurrence of Radon in the Drinking Water of Dehradun City, India", Indoor and Built Environment, 01/01/1999 Publication	<1 %
35	jhygiene.muq.ac.ir Internet Source	<1 %
36	www.groundwatergovernance.org Internet Source	<1 %

37	Sang Jun Sim, Chang Duk Kang, Jin Won Lee, Woo Sik Kim. "TREATMENT OF HIGHLY POLLUTED GROUNDWATER BY NOVEL IRON REMOVAL PROCESS", Journal of Environmental Science and Health, Part A, 2006 Publication	<1 %
38	Sudhir Mittal, Asha Rani, Rohit Mehra. "Estimation of radon concentration in soil and groundwater samples of Northern Rajasthan, India", Journal of Radiation Research and Applied Sciences, 2016 Publication	<1 %
39	coek.info Internet Source	<1 %
40	sciresol.s3.us-east-2.amazonaws.com Internet Source	<1 %
41	www.zancojournals.su.edu.krd Internet Source	<1 %
42	"Outer Himalaya Zone", Physics and Chemistry of the Earth, 1992 Publication	<1 %
43	Abdurabu, Wedad Ali, Ahmad Termizi Ramli, Muneer Aziz Saleh, and Arien Heryansyah. "The activity concentrations of 222Rn and corresponding health risk in groundwater samples from basement and sandstone	<1 %

aquifer; the correlation to physicochemical parameters", Radiation Physics and Chemistry, 2016.
Publication

44	E Babatope Faweya, O Gabriel Olowomofe, H Taiwo Akande, T Adeniyi Adewumi. "Radon emanation and heavy-metals assessment of historical warm and cold springs in Nigeria using different matrices", Environmental Systems Research, 2018 Publication	<1 %
45	Martin Weidenboörner. "Acha", Mycotoxins in Foodstuffs, 2008 Publication	<1 %
46	Nisar Ahmad, Javed Rehman, Jalil ur Rehman, Gulfam Nasar. " Assessments of Ra and Rn concentration in well and tap water from Sik, Malaysia, and consequent dose estimates ", Human and Ecological Risk Assessment: An International Journal, 2019 Publication	<1 %
47	Rita Crasta, Sushma Devadiga, Nikhita Narendra Savant, Vibha Vinayak Naik, Suresha Suresh, Kamalakar Vaijinathrao Dawalekar. "Analysis of radon concentrations in drinking water in coastal regions of Karnataka, South India", Radiation Protection Dosimetry, 2023 Publication	<1 %

48	Sumit Sharma, Ajay Kumar, Rohit Mehra, Ranbir Kaur. "INGESTION AND INHALATION DOSES DUE TO INTAKE OF RADON IN DRINKING WATER SAMPLES OF AMRITSAR PROVINCE, PUNJAB, INDIA", Radiation Protection Dosimetry, 2019 Publication	<1 %
49	documents.deq.utah.gov Internet Source	<1 %
50	ejol.ethernet.edu.et Internet Source	<1 %
51	sci.mu.edu.iq Internet Source	<1 %
52	www.asrjetsjournal.org Internet Source	<1 %
53	www.elftsv.hu Internet Source	<1 %
54	www.hindawi.com Internet Source	<1 %
55	Ajay Kumar, Sumit Sharma, Rohit Mehra, Priya Kanwar, Rosaline Mishra, Inderpreet Kaur. "Assessment of radon concentration and heavy metal contamination in groundwater of Udhampur district, Jammu & Kashmir, India", Environmental Geochemistry and Health, 2017	<1 %

Publication

56	Breure, Mirjam S.. "Models for Predicting Nutrient Availability in Soils from Sub-Saharan Africa", Wageningen University and Research, 2023 Publication	<1 %
57	E. Srinivasa, D. R. Rangaswamy, J. Sannappa. "Determination of radon activity concentration in drinking water and evaluation of the annual effective dose in Hassan district, Karnataka state, India", Journal of Radioanalytical and Nuclear Chemistry, 2015 Publication	<1 %
58	I. S. Arvanitoyannis, C. Chalhoub, P. Gotsiou, N. Lydakis-Simantiris, P. Kefalas. "Novel Quality Control Methods in Conjunction with Chemometrics (Multivariate Analysis) for Detecting Honey Authenticity", Critical Reviews in Food Science and Nutrition, 2005 Publication	<1 %
59	Muhammad Zahoor, Farhat Ali Khan, Muhammad Azam. "Bacteriological, inorganic and heavy metal evaluation of drinking water of the specified flood affected areas of Dir (Lower) Pakistan", Desalination and Water Treatment, 2015 Publication	<1 %

60	R. K. Somashekar, P. Ravikumar. "Radon concentration in groundwater of Varahi and Markandeya river basins, Karnataka State, India", Journal of Radioanalytical and Nuclear Chemistry, 2010 Publication	<1 %
61	DIANE MAROTTA. "NONLINEAR EFFECTS OF GLUTAMATE AND KCl ON GLUTAMATE TOXICITY IN CULTURED RAT CEREBELLAR NEURONS", International Journal of Neuroscience, 4/1/2003 Publication	<1 %
62	IFMBE Proceedings, 2009. Publication	<1 %

Exclude quotes	Off	Exclude matches	Off
Exclude bibliography	Off		